Sedimentary Geology xxx (2016) xxx–xxx

Contents lists available at ScienceDirect

Sedimentary Geology

journal homepage: www.elsevier.com/locate/sedgeo

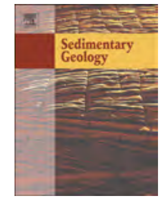

Controls on space–time distribution of soft-sediment deformation structures: Applying palaeomagnetic dating to approach the *apparent recurrence period of* paleoseisms at the Concud fault (eastern Spain)

L. Ezquerro [a,]*, M. Moretti [b], C.L. Liesa [a], A. Luzón [a], E.L. Pueyo [c], J.L. Simón [a]

[a] *Departamento de Ciencias de la Tierra, Universidad de Zaragoza, Pedro Cerbuna 12, 50009 Zaragoza, Spain*
[b] *Dipartimento di Scienze della Terra e Geoambientali, Università degli Studi di Bari, via E. Orabona 4, 70100 Bari, Italy*
[c] *Instituto Geológico y Minero de España, Unidad de Zaragoza, C/Manuel Lasala 44, 50006 Zaragoza, Spain*

A R T I C L E   I N F O

Article history:
Received 27 November 2015
Received in revised form 6 June 2016
Accepted 10 June 2016
Available online xxxx

Keywords:
Soft-sediment deformation structure
Seismites
Seismogenic fault
Magnetostratigraphy
Recurrence period
Jiloca Basin

A B S T R A C T

This work describes soft-sediment deformation structures (clastic dykes, load structures, diapirs, slumps, nodulizations or mudcracks) identified in three sections (Concud, Ramblillas and Masada Cociero) in the Iberian Range, Spain. These sections were logged from boreholes and outcrops in Upper Pliocene-Lower Pleistocene deposits of the Teruel-Concud Residual Basin, close to de Concud normal fault. Timing of the succession and hence of seismic and non-seismic SSDSs, covering a time span between ~3.6 and ~1.9 Ma, has been constrained from previous biostratigraphic and magnetostratigraphic information, then substantially refined from a new magnetostratigraphic study at Masada Cociero profile. Non-seismic SSDSs are relatively well-correlated between sections, while seismic ones are poorly correlated except for several clusters of structures. Between 29 and 35 seismic deformed levels have been computed for the overall stratigraphic succession. Factors controlling the lateral and vertical distribution of SSDSs are their seismic or non-seismic origin, the distance to the seismogenic source (Concud Fault), the sedimentary facies involved in deformation and the observation conditions (borehole core vs. natural outcrop). In the overall stratigraphic section, seismites show an apparent recurrence period of 56 to 108 ka. Clustering of seismic SSDSs levels within a 91-ka-long interval records a period of high paleoseismic activity with an apparent recurrence time of 4.8 to 6.1 ka, associated with increasing sedimentation rate and fault activity. Such activity pattern of the Concud Fault for the Late Pliocene-Early Pliocene, with alternating periods of faster and slower slip, is similar to that for the most recent Quaternary (last ca. 74 ka BP). Concerning the research methods, time occurrence patterns recognized for peaks of paleoseismic activity from SSDSs in boreholes are similar to those inferred from primary evidence in trenches. Consequently, *apparent recurrence periods* calculated from SSDS inventories collected in borehole logs close to seismogenic faults are comparable to actual recurrence times of large paleoearthquakes.

1. Introduction

The use of soft-sediment deformation structures (SSDSs) induced by ground shaking generated by seismic wave (seismites) as a record of past earthquakes is a common practice in sedimentological/stratigraphical (Allen, 1986) and paleoseismological studies (Obermeier, 1996), particularly in ancient to present-day fluvial-lacustrine successions (e.g. Sims, 1975; Davenport and Ringrose, 1987, 1975; Guiraud and Plaziat, 1993; Van Loon et al., 1995; Alfaro et al., 1997; Rodríguez-Pascua et al., 2000; Migowski et al., 2004; Moretti and Sabato, 2007; Moretti and Ronchi, 2011; Stárková et al., 2015). After the innovative work by Sims (1975), many authors have tried to evaluate the recurrence time of past earthquakes by analyzing the vertical repetition of deformed beds in lacustrine successions. Nevertheless, this approach involves some limitations (Montenat et al., 2007; Owen et al., 2011; Moretti and van Loon, 2014) related with the fact that some earthquakes may not be recorded in the sedimentary succession (Moretti et al., 1999) or that a single seismic shock can induce superimposed deformed beds (Gibert et al., 2011).

Recently, after recognizing 21 seismite levels in a 75-m-long borehole through Upper Pliocene-Lower Pleistocene lacustrine deposits of the Teruel Basin (Masada Cociero site), Ezquerro et al. (2015) have proposed the concept of *apparent recurrence period*, as the inverse of the frequency of occurrence of seismites per unit time along a borehole. The term 'apparent' refers to the fact that the paleoseismic record at a given point is a partial one, since the spatial distribution of SSDSs produced by an individual event (and so its probability of being

* Corresponding author. Tel.: +34 976 76 10 81; fax: +34 976 86 11 06.
E-mail address: lope@unizar.es (L. Ezquerro).

http://dx.doi.org/10.1016/j.sedgeo.2016.06.007
0037-0738/© 2016 Elsevier B.V. All rights reserved.

represented at a given site) is limited. In this way, after accepting that subsidence and sedimentation rates were fairly similar, Ezquerro et al. (2015) have estimated an apparent recurrence period of about 45–51 ka for the Masada Cociero borehole log. They also discussed the quality and representativeness of observations of SSDSs in well cores by comparing them with those in natural outcrops. The latter have the advantage of lateral continuity, hence the feasibility for recognizing large-scale SSDSs, whereas well cores, virtually continuous along the entire sedimentary succession, allow detailed observations of fresh rock at a millimeter scale. Reconstructing the paleoseismic record of an area can benefit from combining both data sources, especially if that information from multiple wells is available, allowing correlation of deformed levels in the subsoil. This work goes deeper into this issue, revisiting the same area within the central Teruel Basin (Fig. 1), collecting new surface and subsoil data, and combining multiple research lines in order to reconstruct both the lateral and vertical distribution of SSDSs.

First, a new borehole drilled at Ramblillas site, west of Masada Cociero, together with a new surface profile surveyed close to Concud village (see location in Fig. 2), have enlarged our SSDSs record in the Upper Pliocene-Lower Pleistocene succession. Since the Masada Cociero section also combines a well log and a surface profile, the final available SSDSs inventory adequately combines both data sources.

Second, we have improved the temporal framework of the paleoseismic occurrences. The age of the Masada Cociero succession was constrained by (i) overall correlation with regional lithostratigraphical units, biostratigraphically by numerous mammal sites and a few magnetostratigraphic profiles (one of them at the Concud section; Opdyke et al., 1997), and (ii) a mammal site (*Rotonda Teruel-Centro*, *RTC*; MN 17 zone) located at the Masada Cociero surface profile, which dates these materials to the middle Villafranchian (Ezquerro et al., 2012b). We now add a new magnetostratigraphic study of the Masada Cociero well log, which refines the chronostratigraphy of the studied deposits and provides a more robust correlation of the three surveyed sections. This allows the lateral continuity of deformation structures associated to each paleoseismic event to be assessed, as well as obtaining their precise time distribution along the surveyed profiles, and thus a better calculation of the apparent recurrence period.

The central Teruel Basin is a perfect target for this kind of study since: i) the instrumental and historical seismicity are well-known; ii) the Late Pliocene-Early Pleistocene is recorded by a thick, continuous alluvial-palustrine-lacustrine succession, suitable for dating by magnetostratigraphic methods; and iii) the structure and paleoseismicity of the most active fault in the area, the Concud Fault, are well known (Moissenet, 1983; Simón, 1983; Gutiérrez et al., 2008; Lafuente, 2011; Lafuente et al., 2011a, 2014; Simón et al., 2012, 2015; Ezquerro et al., 2014b).

Our objectives are: (i) to describe the SSDSs that occur at various stratigraphic levels in the Concud-Teruel area, both in outcrops and well logs; (ii) to distinguish seismically from non-seismically induced SSDSs; (iii) to establish the time distribution of SSDSs in different stratigraphic sections, achieving reliable correlations between deformed beds; and iv) to calculate the *apparent recurrence period* of paleoseismic events and discuss the significance of the results.

2. Geological setting

The study area extends along a section transverse to the Concud Fault, which is located at the junction of the Teruel and Jiloca grabens, in the NE of the Iberian Peninsula (Fig. 1a). These basins represent the most landward structures developed within the Iberian Plate in relation to Neogene rifting at the Valencia Trough, Mediterranean Sea (Álvaro et al., 1979; Simón, 1983; Capote et al., 2002). They evolved through two distinct rift episodes (Simón, 1982, 1983): the first one gave rise to the Teruel Graben (NNE–SSW trend) during the Late Miocene, and the second produced the NNW–SSE trending Jiloca Graben and reactivated the Teruel Graben in the Late Pliocene-Quaternary (Capote et al., 2002).

The northern sector of the Teruel Basin is a half graben with an active eastern boundary formed by a NNW–SSE and NNE–SSW trending fault system (Fig. 1b). The basin fill comprises Upper Miocene to Lower Pleistocene deposits whose age is well constrained by abundant mammal sites and magnetostratigraphic profiles (e.g. Adrover et al., 1978;

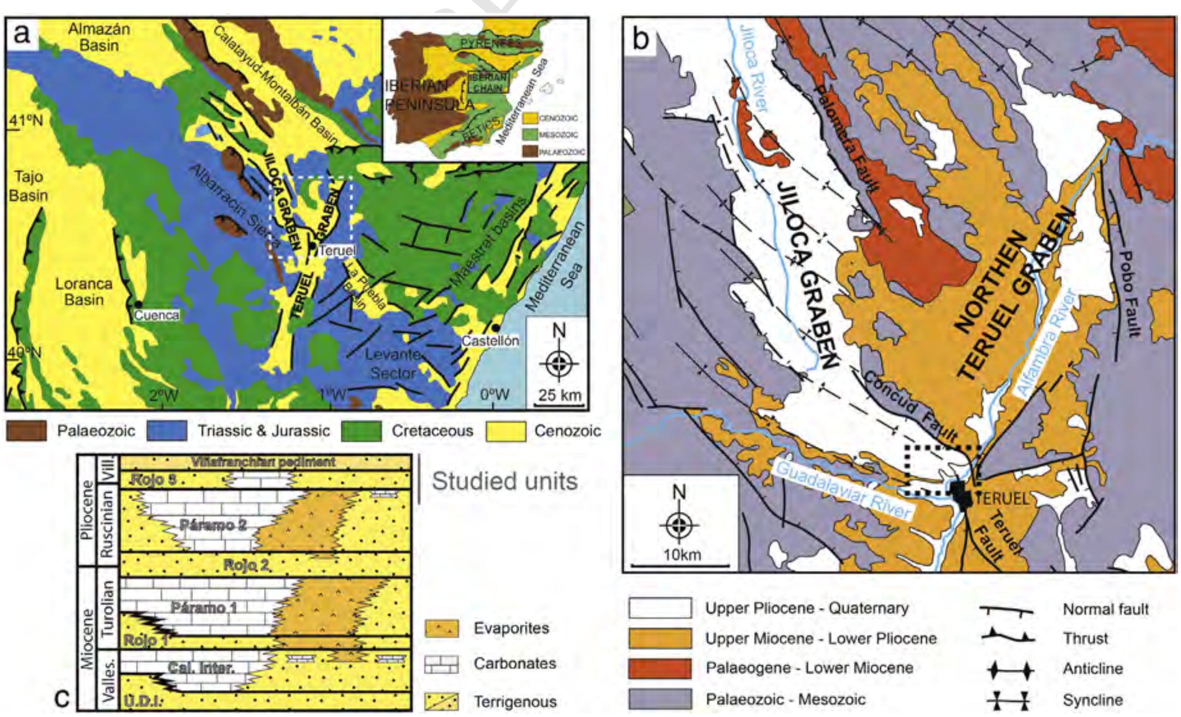

Fig. 1. (a) Neogene-Quaternary extensional basins and the main active faults in the central-eastern Iberian Chain. Inset: location of the study area within the Iberian Peninsula. (b) Geological map of the Jiloca and Teruel basins, with location of the studied area. (c) Stratigraphic units by Godoy et al. (1983a, 1983b).

Adrover, 1986; Mein et al., 1983, 1990; Alcalá et al., 2000; Krijgsman et al., 1996; Opdyke et al., 1997; Garcés et al., 1999; van Dam et al., 2001; van Dam, 2006). The succession comprises endorheic red clastic alluvial deposits ~500 m-thick that grade laterally into lacustrine carbonate and gypsum deposits (Weerd, 1976; Godoy et al., 1983a, 1983b; Moissenet, 1980; Alcalá et al., 2000; Alonso-Zarza and Calvo, 2000; Alonso-Zarza et al., 2012; Ezquerro et al., 2012a, 2014a) divided the basin infill into eight lithological units (Fig. 1c) based on the alternation of carbonate (*Calizas Inferiores*, *Páramo 1* and *Páramo 2*) and terrigenous (*Unidad Detrítica Inferior*, *Rojo 1*, *Rojo 2* and *Rojo 3*) units; this succession culminates with a thin alluvial unit (*Villafranchian pediment*). These units have traditionally been used in national geological maps and represent the initial temporal framework for our purposes.

The asymmetric Jiloca Graben is limited in the East by a NNW–SSE *en-echelon* normal fault system (from north to south: Calamocha, Palomera and Concud faults), the Concud Fault being the southernmost structure (Fig. 1b). The infill features are less well known than in the Teruel Basin as only a 70 m-thick succession crops out located towards the South. Several boreholes in the area indicate that the infill reaches up to 130 m northwards (Rubio and Simón, 2007). The age of the uppermost deposits infilling the endorheic basin prior to the incision of the present-day fluvial network, is well constrained to the Late Pliocene-Early Pleistocene from several mammal sites and magnetostratigraphic profiles (e.g. Mein et al., 1983, 1990; Opdyke et al., 1997; van Dam, 2006; Ezquerro et al., 2012b, 2015). The scarce outcrops in combination with subsurface data indicate that interbedded alluvial fan and palustrine deposits filled the basin, equivalent to the *Páramo 2*, *Rojo 3* and *Villafranchian pediment* units defined in the Teruel Basin (Moissenet, 1982; Rubio and Simón, 2007; Ezquerro et al., 2012b, 2015).

The linkage of the Teruel and Jiloca grabens occurred during the Late Pliocene (~ 3.6 Ma), when the Concud Fault developed (Simón, 1983). The fault has a length of ca. 14.2 km, dip 65° to 70°W, and a general NW–SE strike, which veers to NNW–SSE towards the southern tip, where the Jiloca Graben articulates with the Teruel Graben. Sedimentation was interrupted in the footwall (Teruel Basin) at the end of deposition of the *Páramo 2* unit (Godoy et al., 1983a, 1983b) when the depocentre migrated to the north, towards the Pobo Fault. In the hanging-wall block (Jiloca Basin), lacustrine-palustrine sedimentation was restricted to a small subsiding area close to the Concud Fault surface, the Concud-Teruel Residual Basin (e.g. Moissenet, 1982; Lafuente et al., 2011b; Ezquerro et al., 2012b, 2015). These deposits connected upstream with the distal sectors of alluvial fans fed from the west (Ezquerro et al., 2012b). These sediments correspond to the *Rojo 3* + *Villafranchian Pediment* units (Godoy et al., 1983a, 1983b). During the Early Pleistocene, the hydrological regime changed in both basins to exorheic conditions (Ezquerro et al., 2012b). The Miocene–Pliocene deposits were dissected whereas short alluvial fans and three fluvial terrace levels developed (Godoy et al., 1983a, 1983b; Peña et al., 1984).

The Concud Fault is the main active structure in the area, and the boreholes and outcrops surveyed for this work are located very close (0.2 to 2.0 km) to its trace (Fig. 2a); therefore, it should be considered as the main source for the paleoseisms interpreted from SSDSs. Recent paleoseismological studies of Quaternary deposits affected by the Concud Fault have recognized eleven events between ca. 74 ka BP and the present day (e.g., Lafuente, 2011; Lafuente et al., 2011b, 2014; Simón et al., 2015). The average recurrence period has been calculated as between 7.1 ± 3.5 and 8.0 ± 3.3 ka, with a total net accumulated slip of about 20.5 m and an average coseismic slip of 1.9 m. The displacement pattern shows alternating periods of faster slip (up to 0.53 mm/a) and slower slip (0.13 mm/a), resulting in an average slip rate of 0.29 mm/a. The characteristic earthquake at the Concud Fault is estimated at Mw = 6.5–6.6 (Ezquerro et al., 2015; Simón et al., 2015).

The Teruel Fault is a second potential seismogenic source in the area; it exhibits a 9 km-long trace, and its characteristic earthquake is estimated at Mw = 6.1–6.6 (Simón et al., in press). Our studied sites are located at distances of 1.8 to 4.4 from this fault. This structure was initiated ~3.6 Ma ago, as a blind fault south of Teruel city, then propagated upwards and northwards up to acquiring its present-day trace. A hypothetic propagation towards the study area could occur after Middle Pleistocene time (Lafuente et al., 2011b; Simón et al., in press). Therefore, for the studied succession and time interval (Late Pliocene-Early Pleistocene), the Teruel Fault was smaller and farther than the Concud Fault, so it could only represent a minor seismic source.

3. Sedimentary succession of the Concud-Teruel Residual Basin

The characterization of the sedimentary succession of the Late Pliocene Concud-Teruel Residual Basin is mainly derived from three detailed stratigraphic sections studied in the field (Masada Cociero, Ramblillas and Concud sections), as well as a log of continuous cores recovered in two wells (Masada Cociero and Ramblillas). Combination of surface and subsurface information has allowed the construction of three complete stratigraphic profiles from different sectors of the basin, as well as a facies associations map (Fig. 2). In the eastern sector, the basin infill consists of a syn-tectonic palustrine-lacustrine succession, comprising silty carbonates, marls, limestones and coal beds, that progressively passes towards the west into alluvial deposits comprising mudstones, sandstones and conglomerates (see Ezquerro et al., 2012b, 2015).

The Masada Cociero profile (1 in Fig. 2) was described in detail by Ezquerro et al. (2012b, 2015). It is a composite profile located close to the Concud Fault that comprises a 13.7 m-thick outcropping succession and a 75 m-thick subsurface succession drilled at the bottom of the outcrop. A gap of 12 m due to the Alfambra River incision and Quaternary sedimentation interrupts continuity between both. The lower part of the succession consists of whitish carbonate and evaporite deposits that grade up into reddish mudstones and darkish silts; the succession is more terrigenous towards the top, with mudstones and occasional intercalations of brown sandstones and red conglomerates, but a carbonate-dominated part can be recognized towards the middle of the profile. The *RTC* mammal site (MN 17 zone), Middle Villafranchian in age (Ezquerro et al., 2012b), is situated at the base of the outcropping series (see Fig. 2). These sediments mainly correspond to the *Rojo 3* unit of Godoy et al. (1983a, 1983b), although the whitish carbonate and evaporite deposits at the base of the well log could correspond to the pre-tectonic *Páramo 2* unit. A new magnetostratigraphic profile has been made to constrain the age of this succession (see below).

As in the previous case, the 45.6 m-thick Ramblillas composite profile (2 in Fig. 2) includes a 5.4 m-thick outcropping succession and a 40.2 m-thick subsurface succession drilled at the bottom of the outcrop. The basal deposits are pale-colored carbonate silts, darkish marls and red mudstones. Above them, the succession is dominantly clastic (orange mudstones and sandstones), but some interbedded carbonate (darkish marls and whitish silts) and brown conglomerate beds also appear. The profile corresponds to the *Rojo 3* unit of Godoy et al. (1983a, 1983b) except for the upper part of the section, where a tabular body of grayish conglomerates has been ascribed to the *Villafranchian pediment* unit (Ezquerro et al., 2012b). This distinctive body has also allowed the physical correlation with the Concud profile (Fig. 3). According to regional data, its age can be attributed to the Late Pliocene (~ 3.0–2.1 Ma).

The Concud profile (3 in Fig. 2) was entirely logged from outcropping materials and comprises a 49.8 m-thick succession conformably lying on the whitish limestones and marlst of the *Páramo 2* unit (Godoy et al., 1983a, 1983b). Its lower part (0 to 24 m) is very heterogeneous, with carbonate deposits, mainly tabular beds of darkish marls, whitish silts, and grayish limestones, orange mudstones and sandstones. The upper part (25 to 50 m) is more clastic, being made up of orange mudstone and sandstone tabular strata with scarce marl intercalations. The top of the section consists of grayish conglomerate bodies (tabular or channeled) with intercalated mudstone beds, which have been attributed to the *Villafranchian pediment* unit. The presence

Please cite this article as: Ezquerro, L., et al., Controls on space–time distribution of soft-sediment deformation structures: Applying palaeomagnetic dating to approach the *apparent*..., Sedimentary Geology (2016), http://dx.doi.org/10.1016/j.sedgeo.2016.06.007

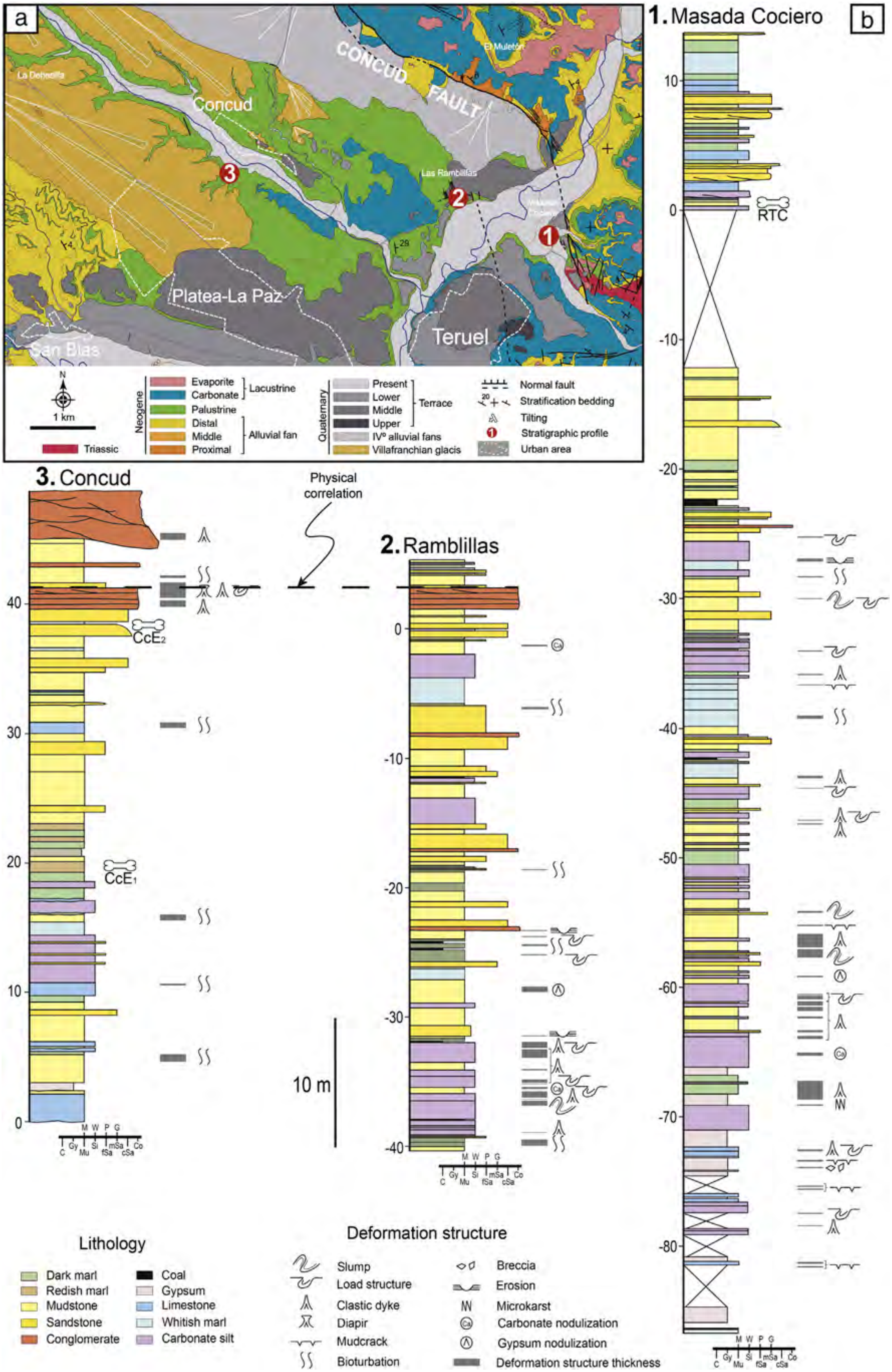

Fig. 2. Stratigraphic profiles along the Concud-Teruel Residual Basin (2 km north of Teruel), see location in Fig. 2a. The Ramblillas and Masada Cociero profiles correspond with composite sections, borehole data and surface data are displaying in negative and positive numbers, respectively.

Please cite this article as: Ezquerro, L., et al., Controls on space–time distribution of soft-sediment deformation structures: Applying palaeomagnetic dating to approach the *apparent*..., Sedimentary Geology (2016), http://dx.doi.org/10.1016/j.sedgeo.2016.06.007

of the *Concud Estación* mammal site (MN 16 zone) of Early Villafranchian age (Mein et al., 1990) and the Concud magnetostratigraphic profile (Opdyke et al., 1997) allow the age of this profile to be bracketed between 3.0 and 2.1 Ma.

4. Paleomagnetic study of the Masada Cociero profile

Magnetostratigraphy is a good method for dating sedimentary
Q8 sequences (Opdyke and Channell, 1996). The reconstruction of a reliable local polarity sequence (LPS) allows comparison to the Global Polarity Time Scale (GPTS) and dating of polarity boundaries found in that sequence. This brackets the resolution of the method but still permits the identification of a number of isochrones in the stratigraphic record. Previous studies in the basin (Krijgsman, 1996; Krijgsman et al., 1996; Opdyke et al., 1997; Sinusía et al., 2004) make us confident about the suitability of this technique to provide a temporal constraint in our study.

The paleomagnetic study was performed in the Masada Cociero succession, aiming to find as many magnetozones as possible, searching for an independent calibration to the GPTS and thus, the dating of the studied section. This profile was selected due to: i) the availability of the *RTC* mammal site (MN17 zone) to help in the correlation with the Concud magnetostratigraphic profile (Opdyke et al., 1997); ii) the occurrence of a large number of SSDSs; and iii) the possibility of establishing a temporal model for the distribution of SSDSs to clarify their environmental significance. In this section, only the main results concerning the paleomagnetic components, the establishment of the Local Polarity Sequence (LPS), and its correlation to the Global Polarity Time Scale (GPTS) will be discussed. Sampling and laboratory procedures, rock magnetism demagnetization results and details on the Characterisctic Remanent Magnetizations (ChRM) are included in Appendix A.

4.1. Paleomagnetic components

The intensity of the Natural Remanent Magnetization (NRM) spreads from weak values ($< 100 \cdot 10^{-6}$ A/m) to relatively high ones ($30.000 \cdot 10^{-6}$ A/m), although ~76% of the distribution displays intensities above 1 mA/m and 18% below 0,1 mA/m (Fig. 3). The demagnetization of the NRM shows the occurrence of relatively simple and noisy paths. The paleomagnetic signal is slightly scattered, which is related to the diversity of rock types and their variable magnetic stability. A remarkable difference in NRM intensities is observed, up to three orders of magnitude higher in reddish mudstones, marls and sandstones than in limestones, carbonate silts and gypsums (Fig. 3). The Isothermal Remanent Magnetization (IRM) acquisition curves outline the contribution of different magnetic minerals to the remanence. The remanence in Masada Cociero is mainly carried by magnetite, although iron sulfides and hematite also contribute in some cases (Appendix A).

A secondary low-temperature Viscous Remanent Magnetization (VRM) has been observed in most samples. The VRM component is unblocked in the 20–200 °C interval, but in some samples it can be tracked up to 300–350 °C and contributes to the noisy pattern observed. Apart from a viscous component, 43% of samples showed intermediate unblocking temperatures up to 550 °C. Finally, a high temperature component is dominant (57% of samples) and can be tracked up to 660–680 °C. The Characteristic Remanent Magnetization (ChRM) has been always defined in these last two unblocking intervals and, as a general rule, normal and reverse polarity samples tend to address the coordinate origin in the orthogonal diagrams (Appendix A).

The secondary low-temperature VRM component is assumed to record the present-day field and is therefore a potential tool for orienting the samples recovered from the rotation-drilling core (Fuller, 1969; Bleakly et al., 1985; Stokking et al., 1993; Thibal et al., 1999; Zhang et al., 2007). This assumption is confirmed by analyzing oriented samples collected from outcropping rocks at the upper part of the profile: the VRM direction (declination 033°, inclination 56°; α_{95}: 14.7°, k: 3.2 and R: 0.7022) is not far from the present-day geomagnetic field (355°, 56°) deduced from the NOAA's National Geophysical Data Center using the IGRF12-gufm1 model (Jackson et al., 2000). Accordingly, the samples from the well core were oriented using the VRM direction (thermal interval) to the present-axial-dipole field (Fuller, 1969; Van der Voo and Watts, 1978; Shibuya et al., 1991; Hailwood and Ding, 1995). The only disadvantage of this method is the transference of the fisherian noise of the VRM to the ChRM direction. The pseudoantipodality found between the normal and reverse means in our dataset after the correction validates the re-orientation methodology used in this work (Appendix A), although steepening of the vectors induced by the coring of the well cannot be ruled out.

4.2. Local polarity sequence (LPS)

The absence of original orientations prevents us applying more rigorous filtering methods (Deenen et al., 2011) to build a sound and reliable LPS. Therefore, we have classified the ChRM directions into three groups to avoid unnecessary noise in the LPS: class I samples (30% of samples) are reliable directions addressed to the origin; class II samples (40%) are poorer quality directions but polarity is unambiguous; class III (30%) includes the remaining (low-quality) set of samples, which were not used in any further processing of the data (Appendix A). The Masada Cociero LPS is based on 180 reliable samples, which represent about 60% of successful demagnetizations (Fig. 4). The consistency of the constructed LPS is also founded on the magnetozone pattern: as will be shown later, ChRM from classes I and II were used to calculate the paleo-latitude of the Virtual Geomagnetic Pole (VGP). Despite the slightly noisy signal and the moderate quality of the magnetization, all these criteria help to build a consistent and reliable LPS in which 8 different magnetozones were recognized (Fig. 4).

The profile starts with a reversed zone (R1), which spreads along 9 m with 3 levels of class I. Despite the small number of levels with reliable polarity, almost 20 reversed polarity levels of low quality also fall this magnetozone. N1 starts just above, and covers 8.5 m (5 consecutive levels). R2 is developed between −70 to −68 m (two class I levels). N2 spans along the next 16.4 m. R3 occurs from −51.6 to −49.5 m and is defined by one class I level together to several levels of class II. N3 represents 20.5 m; despite the density of samples in this portion of the profile, some noise prevents a clearer definition of this zone, although the dominance of the normal polarity cannot be questioned. In the R4 local zone (from −28 to 7.4 m) the reverse dominant polarity is punctually obscured by a few normal samples. Unfortunately, the middle part of R4 is not represented; as explained in Section 3, it is substituted in the upper part of the Masada Cociero well core by a 12 m-thick succession of clastic fluvial facies, corresponding to a Pleistocene fluvial terrace incised in Pliocene sediments (Ezquerro et al., 2015). The strong inconsistency with the LPS is corroborated by the highly grouped declinations and normal polarity close to 50° of inclination obtained for samples from such upper sediments (likely Bruhnes magnetic period). Right on top of R4, the uppermost magnetozone (N4) can be more clearly delineated with 6.3 m (4 levels) of normal polarity just below the end of the profile. N3 and R4 represent the noisiest portion of the Masada Cociero LPS.

4.3. Correlation of the Masada Cociero LPS to the GPTS

Once the Masada Cociero LPS has been built, its integration with the biostratigraphic assignation of the *RTC* mammal site and other additional constraints help to propose a reasonable correlation with the GPTS (Ogg, 2012). Following Ezquerro et al. (2012b), the mammal fauna association at the *RTC* site (e.G. *gazella borbonica*, *Stephanorhinus etruscus* and *Equus stenonis*) is characteristic of mammal zone MN17 (Mein, 1975). Thus, the presence of *Equus stenonis* determines a Villafranchian age, which is similar to that ascribed for the neighboring (see location in Fig. 1a) classic mammal site of *La Puebla de Valverde* (MN17, Adrover Q9

Please cite this article as: Ezquerro, L., et al., Controls on space–time distribution of soft-sediment deformation structures: Applying palaeomagnetic dating to approach the *apparent*..., Sedimentary Geology (2016), http://dx.doi.org/10.1016/j.sedgeo.2016.06.007

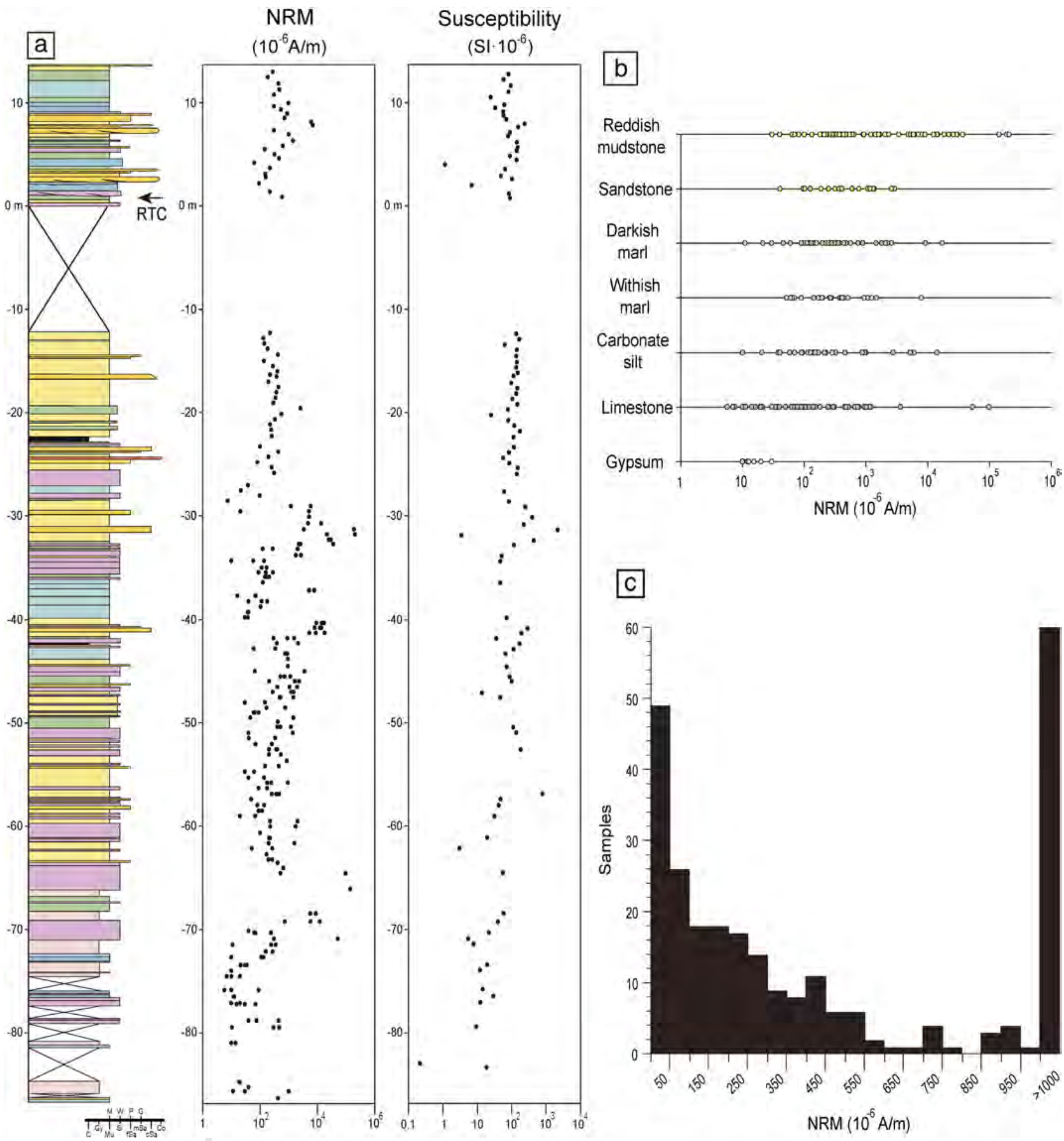

Fig. 3. Magnetic paramenters. Natural remanent magnetization and bulk susceptibility in the Masada Cociero section. NRM has been also plotted against lithology (upper right) and a histogram of NRM and k are also shown (lower right).

et al., 1978), which was analyzed by magnetostratigraphy and correlated with chron C2r.1r (middle Villafranchian, Sinusía et al., 2004). In addition, from mammal site information (e.g. *Concud Estación* site, Mein et al., 1990) and magnetostratigraphic profiling (e.g. Concud profile, Opdyke et al., 1997), our targeted *Rojo 3* and *Villafranchian pediment* units can be dated as Upper Pliocene-Lower Pleistocene. The reader is referred to Fig. 9 by Ezquerro et al. (2012b), in which a compilation of the correlation and ages of these units along the Teruel and Jiloca basins is displayed.

This bio- and magnetostratigraphic frame brackets the time interval represented by the Masada Cociero LPS between the latest Ruscinian and the end of the Villafranchian (Fig. 5). The long reversed portion at the top of the profile (R4) must necessarily belong to the C2r chron (Matuyama), and thus the relation between N4 and C2n seems clear, i.e. the Olduvai subchron. In this way, R4 would correspond to the base of the Matuyama reversed chron. Following this reasoning, N3 + R3 have been correlated with C2An.1 (top of C2An) within the Gauss chron, and N2 + R2 correspond to C2An.2 (middle of C2An).

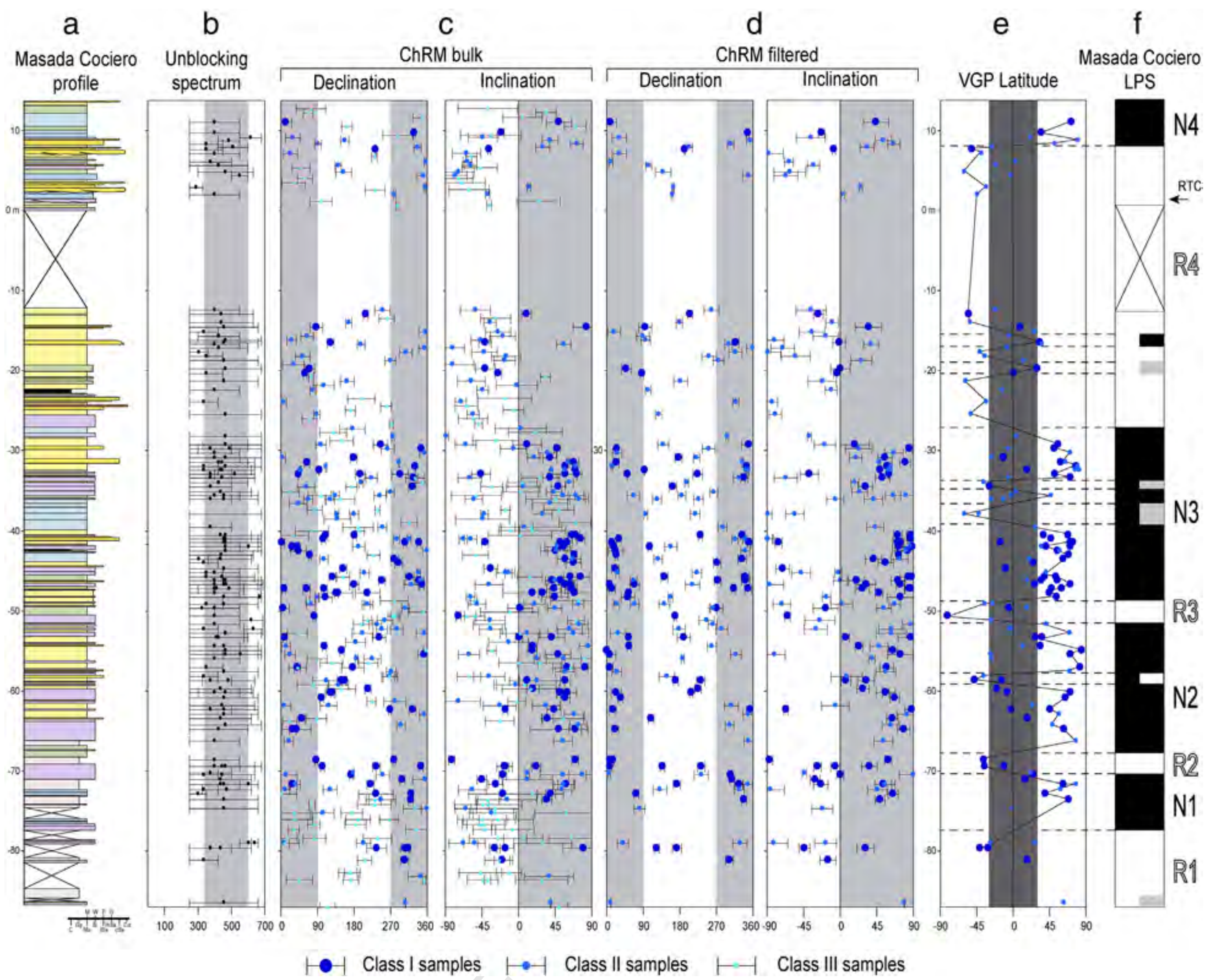

Fig. 4. Magnetostratigraphy in the Masada Cociero composite section; paleomagnetic logs. (a) Lithology. (b) Unblocking spectrum. (c) Declination and inclination of the ChRM of the total samples. (d) Declination and inclination of the ChRM of the total samples. (e) Latitude of the VGP. (f) Local polarity sequence (LPS). Error bars represent the α95 confidence angle. The size of the points refers to the quality of data.

Thus, R3 would be Kaena subchron and, tentatively, R2 the Mammoth one. This later correlation is supported by the longer length and better quality found in R2 against the small reversed interval found between R2 and R3. We believe N3 could correspond to the top of the Gauss normal chron (C2An). Then, the long R1 local zone could be assigned to the top of the long-lasting C2Ar chron (Gilbert reversed chron). According to our interpretation, the base of the Masada Cociero section (R1/N1 boundary) could fit to the C2Ar/C2An, limit located around the Ruscinian-Villafranchian boundary. On the other hand, the unstable normal polarity samples found at the base of R4 could correspond to the Reunion subchron, although the reliability of this local zone is uncertain.

5. Stratigraphic correlation and age of the involved sediments

Stratigraphic correlation of the studied profiles has been mainly based on physical correlation of beds, vertical trend of sedimentary facies, and magnetostratigraphic data (both published and new). The latter have allowed chronological refinement of the studied sediments. Since most of the studied sediments do not crop out, physical correlation of beds was only possible for a tabular conglomerate package located at the upper part of the Concud and Ramblillas profiles (Fig. 6). This 1.5 m-thick tabular deposit has been physically correlated from visual inspection during fieldwork, as well as from analysis of 1:18,000-scale aerial photographs and 1:5000-scale satellite orthoimages.

The vertical trend of sedimentary facies has been used as a powerful tool in the correlation of stratigraphic sequences, especially for siliciclastic units (Posamentier and Allen, 1999). In our case, the construction of the vertical evolution curve has been made using the following procedure:

i) Lithological types were grouped according to their environmental significance, assigning a numerical value that refers to their relative proximal/distal position: alluvial (value 5), mudflat (value 4), palustrine (value 3), shallow lacustrine (value 2) and lacustrine (value 1).
ii) Arithmetic means of such values were calculated for each meter of the stratigraphic succession (values were weighted according to the thickness of each lithological group).
iii) These mean values were smoothed by applying a 3-point moving average.

The curves so obtained, reflecting some alternating episodes of alluvial progradation and lacustrine expansion, has been plotted along the corresponding stratigraphic profiles in Fig. 6. Comparison between profiles has allows the recognition of similar trends between them, which have enabled the correlation of the three successions. Below chron C2r.2r, the proposed correlation is based on the vertical trend curves, so that the maxima (and minima) of the trend curve located in a similar

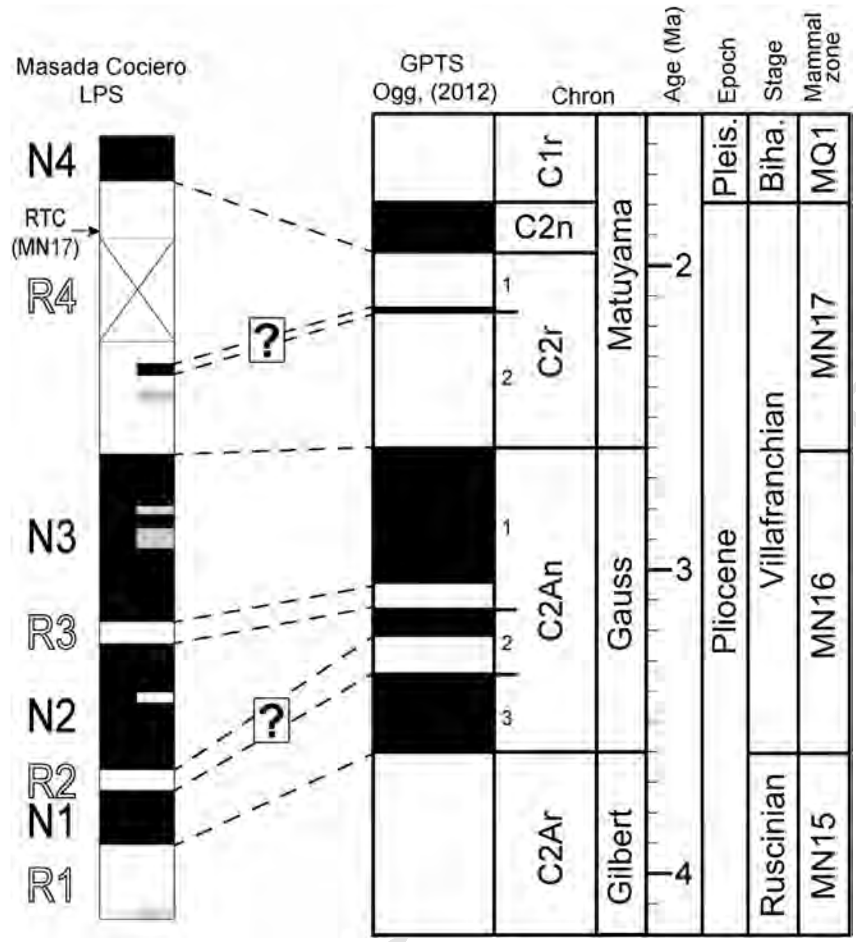

Fig. 5. Correlation of the Masada Cociero LPS with the Global Polarity Time Scale (GPTS) (Ogg, 2012).

stratigraphical position of each succession are considered isochronous. Accordingly, in addition to the basal, pre-tectonic *Páramo 2* unit of the easternmost section, eight sub-units (I to VIII) have been distinguished within the *Rojo 3* unit and the overlying *Villafranchian pediment* unit. Such subunits are not based on simple lithological criteria, but in the vertical trend curve, with each subunit comprising the materials between two consecutive lower values. Overall, the Concud (western) section displays higher absolute values than the Masada Cociero (eastern) section, reflecting the proximal-distal polarity of the sedimentary system.

The magnetostratigraphic results obtained in the Masada Cociero section have allowed us to constrain the age of the sediments. The previously distinguished sub-units range in age between ~3.6 and ~1.8 Ma (Fig. 6). Magnetostratigraphy proposed for the Concud profile by Opdyke et al. (1997), who located the C2An.1-C2r.2 boundary at the upper part of the section (Fig. 6), provides additional constraints and is in accordance with our results in Masada Cociero section. Our study provides greater precision than that conducted by Opdyke et al. (1997), which was carried out with a variable and wider (>5 m) sampling interval. The above-mentioned boundary is now located ca. 3 m lower than the original proposal by Opdyke et al. (1997). The strong constraint of this boundary in our W-E cross-section is the basis for using it as the datum for stratigraphic correlation.

On the other hand, if the thickness of chrons and subchrons recorded in the Masada Cociero LPS is compared with the GPTS, sedimentation rates for the whole studied succession and for each chron and subchron can be displayed and calculated (Fig. 7). The average sedimentation rate for the succession is ca. 0.06 mm/a, i.e. slightly lower than the maximum rate (0.07 to 0.08 mm/a) previously estimated from the total displacement of the top of *Páramo 2* unit (Ezquerro et al., 2015). However, two episodes of, first, lower (0.02 mm/a) and, then, higher (0.13–0.17 mm/a) sedimentation rate affect the lower part of the C2An chron and the whole C2r chron, respectively.

6. Soft-sediment deformation structures

Soft-sediment deformation structures (SSDSs) occur at many stratigraphic levels in the three studied sections, located up to 5 km from the Concud Fault. Detailed descriptions of the SSDSs in the Masada Cociero well core were provided by Ezquerro et al. (2015). More than 35 deformed beds (21 interpreted as seismically-induced) were investigated, allowing the reliability of palaeoseismic studies from the well cores to be assessed. We refer to the work by Ezquerro et al. (2015) for descriptions of deformed beds and interpretations of deformation mechanisms and triggers.

In the present work we describe SSDSs from the Ramblillas well core (similar to those described in the Masada Cociero well core) and from the Concud outcrops. A total of 28 deformed levels have been observed, 20 in the Ramblillas well core and 8 in the Concud section (Fig. 6). The well core has been studied at a millimeter-scale (Figs. 8, 10), whereas in the Concud outcrops centimetric to metric-scale observations were usually made (Fig. 9). Next, we focused on describing SSDSs produced by liquidization and fluidization processes, discarding other SSDSs with authigenic origins, such as pedogenic, mechanic or biologic triggers. The vertical and temporal occurrence along the study succession of these last SSDSs is considered in discussion below. On the basis of lithology, morphology and size of soft-sediment deformation structures, four different types are established: clastic dykes and sills, load

Please cite this article as: Ezquerro, L., et al., Controls on space–time distribution of soft-sediment deformation structures: Applying palaeomagnetic dating to approach the *apparent*..., Sedimentary Geology (2016), http://dx.doi.org/10.1016/j.sedgeo.2016.06.007

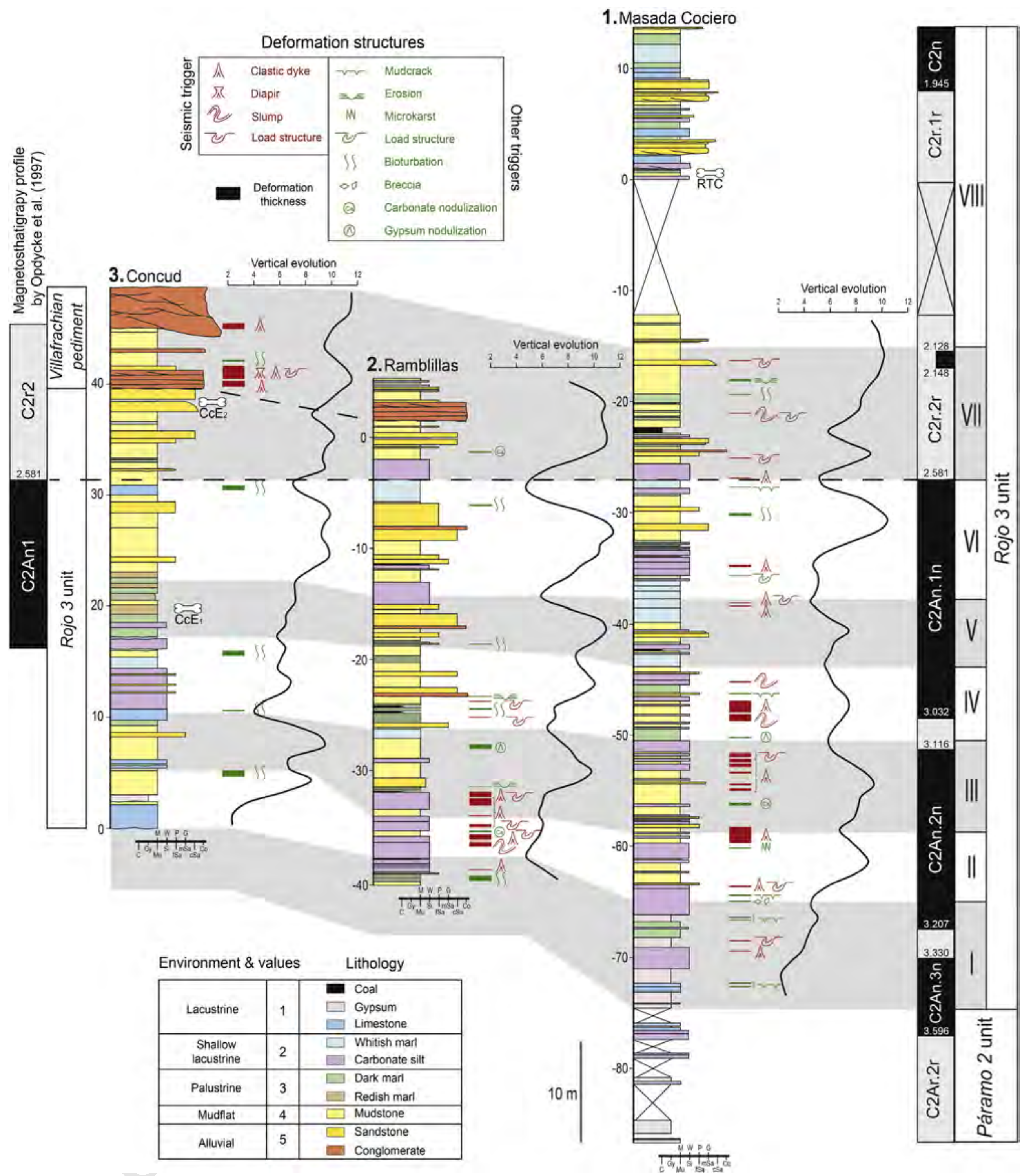

Fig. 6. Correlation of stratigraphic profiles and SSDSs along the Concud-Teruel Residual Basin. The sub-units for the Rojo 3 unit have been defined through vertical trend of sedimentary facies.

structures, slumps and diapirs (Fig. 6). We will distinguish well core and outcrop examples since our descriptions are strongly dependent on the scale of the available observations.

6.1. SSDSs morphology

6.1.1. Clastic dykes

Clastic dykes and dyke-sill complexes appear six times in the Ramblillas well core. They show variable shape in 2D section, but always have a more or less elongated cylindrical 3D morphology. Conduits are dominantly vertical and show sharp contacts with the surrounding materials.

Dykes in core examples are filled by structureless siltstone, silty sandstone and fine-grained sandstone. The host sediments are commonly distorted and folded upwards close to the conduit boundaries (Fig. 8b,d). The size of the vertical conduit is variable, ranging from 0.1 to 1 m in height. Isolated and nearly vertical conduits occur in alternating layers of siltstone and silty sandstone (Fig. 8b). Dyke-sill complexes,

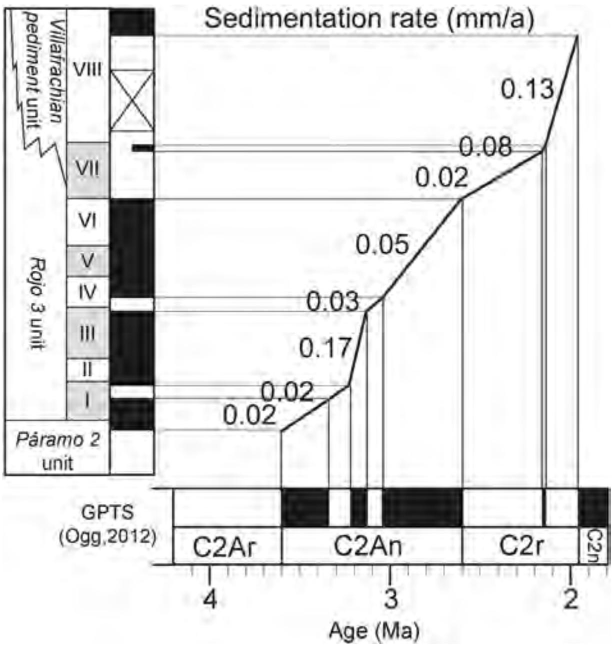

Fig. 7. Variation of sedimentation rate along the Masada Cociero profile.

consisting of vertical, inclined and horizontal conduits, are characteristic of mudstone-siltstone alternations (Fig. 8d). At their upper terminations, some dykes show convex morphologies (under mudstone beds) that slightly deform the overlying fine-grained laminae, while others have upward-widening funnel shapes. Source beds of the clastic dykes always show homogenized texture (Fig. 8c).

Dykes recognized at outcrop (two beds at the uppermost alluvial-lacustrine deposits of the Concud section) are 0.45 to 0.5 m in height and show a laterally and vertically variable length. The upward-directed injections are developed in fine-grained sandstone, siltstone and conglomerate alternations and show irregular morphologies: they are often not vertical (Fig. 9a, b). In some dykes (Fig. 9a), the conduit is filled by coarse-grained reddish siltstone with floating gravels and deforms the adjacent coarse-grained sandstones, which show upward folded lamination. Other dykes only involve coarse-grained sandstones and conglomerates (Fig. 9b). Here, the conduit is filled by sandstone with dispersed gravels and cuts conglomerate beds, deforming them along upward-oriented tight folds (Fig. 9b). Close to the dyke borders, some pebbles have their major axis sub-parallel to the dyke (Fig. 9a,b). The dykes always end upwards at an erosional surface, overlain by undeformed sediments made up of channeled deposits with trough cross-bedding (Fig. 9a) or tabular well stratified gravel bodies with imbricated pebbles (Fig. 9b). Source beds of the clastic dykes always show a massive texture and vertically oriented clasts.

6.1.2. Load structures

In the Ramblillas well core we have recognized four deformed beds with load structures. They have variable heights, from a few centimeters to 0.5 m, but their total length is unknown because their size usually exceeds the diameter of the well log (Fig. 8a,c). They have been recognized as deformed interfaces between two sedimentary units with different lithology or grain-size and are represented by undulations with slight to tight folds with concave/convex morphologies. The overlying unit is made of sandstones or coarse-grained siltstones, while the underlying unit shows a finer grain size (siltstones and mudstones - Fig. 8a,c). In large load structures developed in silty materials, the internal lamination is curved following the structure morphology and, only in the core of the load-structure, laminae are irregularly deformed (Fig. 8c).

In the case of the small-scale load structures, several load casts separated by irregular flame structures can be recognized (Fig. 8a). Locally, the upper sediment moves downwards forming isolated drop-shaped bodies (pillow structures that are a few millimeters in width) in the lower sediment (Fig. 8a).

In the Concud outcrops, large-scale load-structures (more than 0.3 m in length) are associated only with diapirs (see below) in a sandstone-dominated portion of the succession (Fig. 9d).

6.1.3. Diapirs

These structures have only been recognized in a 1.20 m-thick sandstone body in the Concud outcrops. The deposits are made up of alternations of fine- to medium- and coarse-grained sandstone with trough cross-bedding. Several diapir structures occur, reaching a maximum of 0.42 m in height and 0.30 m in length (Fig. 9c). The term diapir is here used to describe dome-shaped SSDSs that arch the overlying laminae without breaking them. In the upper part of the structures, the primary sedimentary lamination is well preserved but shows convexity, regardless of the grain size. In general, they represent symmetrical antiformal folds with angular hinge. The lower zones are made up of fine-grained sandstones, which are massive or show irregularly deformed laminae. Occasionally, some diapirs exhibit a mushroom geometry related to load structures, while others are truncated by an overlying erosional surface (Fig. 9d).

6.1.4. Slumps

Only one 0.40 m thick slump sheet has been recognized in the Ramblillas well core from −36.90 m to −36.50 m (Fig. 10). It involves alternations of grayish and whitish carbonate laminae, brown silts and yellowish coarse-grained silts. Contractional structures such as overturned folds have been recognized (consistent with a single lateral flow direction) even though their size exceeds the well core diameter. A completely distorted bed with folded dykes (brown silty material) appears at the lower part of the slump sheet (Fig. 10). Brown muddy silts with aligned fragments of whitish carbonate and grayish silts picks out a consistently oriented overturned fold (central part of Fig. 10). The uppermost complexly contorted and inclined lamination of grayish silts and mudstones also defines an overturned fold (Fig. 10).

6.2. Causes of deformation

The detailed description of soft-sediment deformation structures allows us to interpret the mechanism of deformation. Liquefaction is responsible for deformation of levels that preserve primary lamination (see Owen and Moretti, 2011). In both load-structures and laminae sets that are passively curved and/or broken by deformation of the adjacent soft-sediments, primary lamination is severely deformed, folded and/or disrupted but is always well recognizable. Fluidization is chiefly recorded by massive textures and upward-directed water-escape structures. Homogenized sediments in the clastic dykes and diapir structures are the result of elutriation of particles from a source bed during fluidization, when water and fluidized particles move upwards deforming the overlying sediments. In the well logs and outcrops, we have often observed the result of a selective-partial fluidization, in which only fine-grained particles made up the upward-directed portions of dykes and diapir structures. Slump sheets are the result of plastic and pseudoplastic deformation in soft-sediments. Being the result of resedimentation and/or slide events, the effects of the initial deformation mechanism (liquefaction, fluidization or a decrease in shear strength) are not recognizable.

The driving-force system (Owen, 1987; Owen et al., 2011) that is responsible for the final morphology of the described Pliocene-Quaternary deformed beds can be summarized as follows: i) load-structures form, after liquefaction, as a result of initial unstable density gradient systems or unequal loading distribution; ii) dykes and diapir structures form after fluidization, where the flow reaches a barrier or

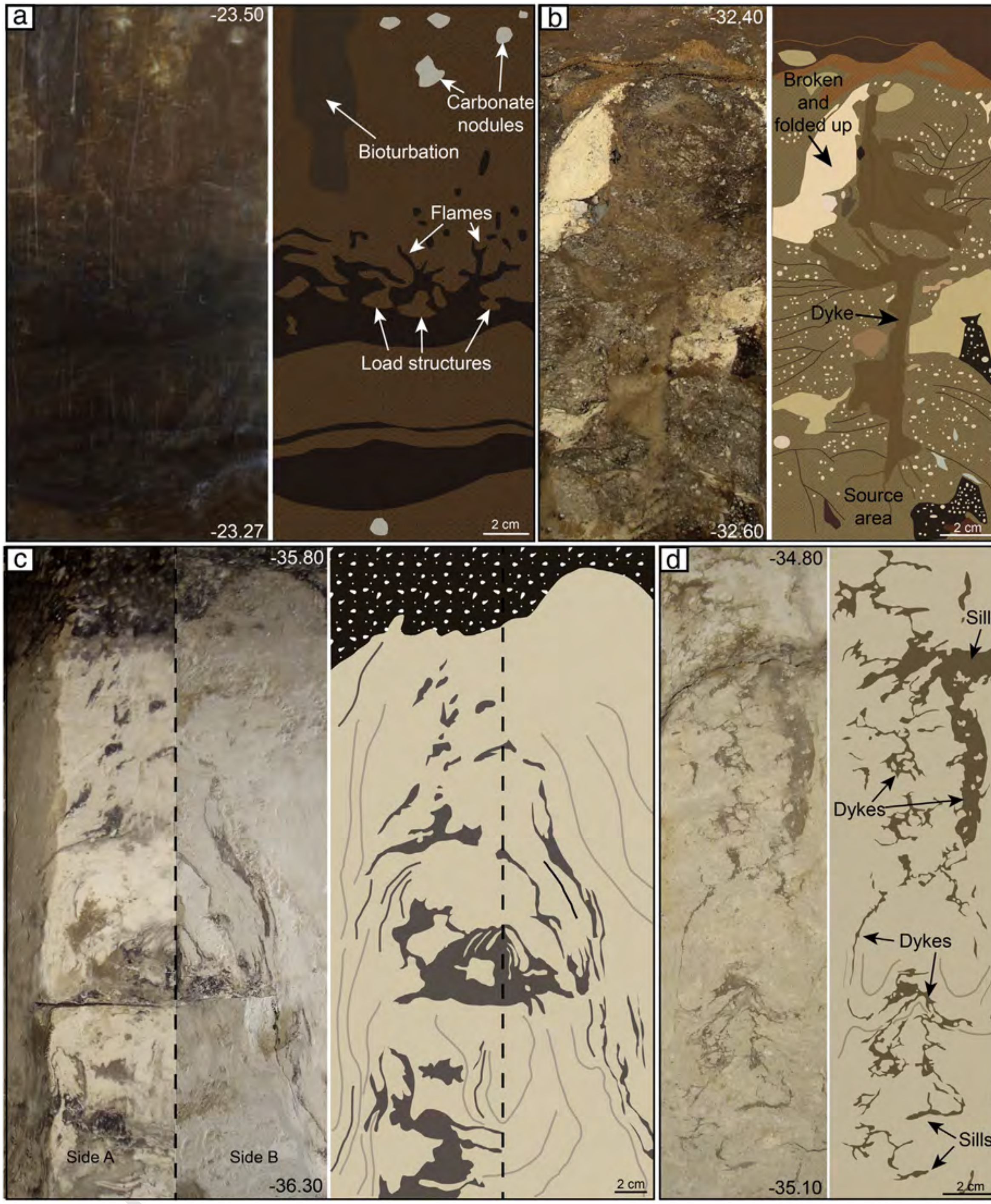

Fig. 8. (a) Load structures (load casts and small pillows) in a centimeter-scale bed, developed in pale-brown and dark-brown silts. Note the presence of bioturbation and carbonate nodules. (b) Clastic dyke: single vertical conduit filled with fine-grained silts and crossing surrounding heterolithic materials (mudstones, limestones and coal). Source bed is shown. (c) Large load-structure only visible between two perpendicular core sections (white silts and brown mudstones). (d) Complex of vertical, inclined and sub-horizontal (sill) dykes related to liquefaction of the brown silty material.

a sharp decrease in permeability; and iii) slump sheets are induced by gravitational instability of a sedimentary body that undergoes liquefaction, fluidization or loss of shear strength.

The interpretation of the trigger mechanism of SSDSs can be often very difficult since many agents can produce very similar morphology (e.g. Dzulynski and Walton, 1965; Lowe, 1975; Eissmann, 1994; Tuttle et al., 2002; Montenat et al., 2007; Van Loon, 2009). Nevertheless, reliable interpretations can be obtained by considering the entire data and results arising from facies analysis and detailed description of SSDSs (e.g. Obermeier et al., 1985; Guiraud and Plaziat, 1993; Moretti, 2000; Owen and Moretti, 2008; Alfaro et al., 2010; El Taki and Pratt, 2012). An exhaustive discussion on how to distinguish seismically-induced SSDSs from aseismic ones in fluvial-lacustrine successions is contained in Moretti and Sabato (2007), while the criteria for recognizing seismites in well logs were systematized by Ezquerro et al. (2015).

The effects of liquefaction and/or fluidization processes on load-structures, dykes and diapir structures of the Pliocene-Quaternary

Please cite this article as: Ezquerro, L., et al., Controls on space–time distribution of soft-sediment deformation structures: Applying palaeomagnetic dating to approach the *apparent*..., Sedimentary Geology (2016), http://dx.doi.org/10.1016/j.sedgeo.2016.06.007

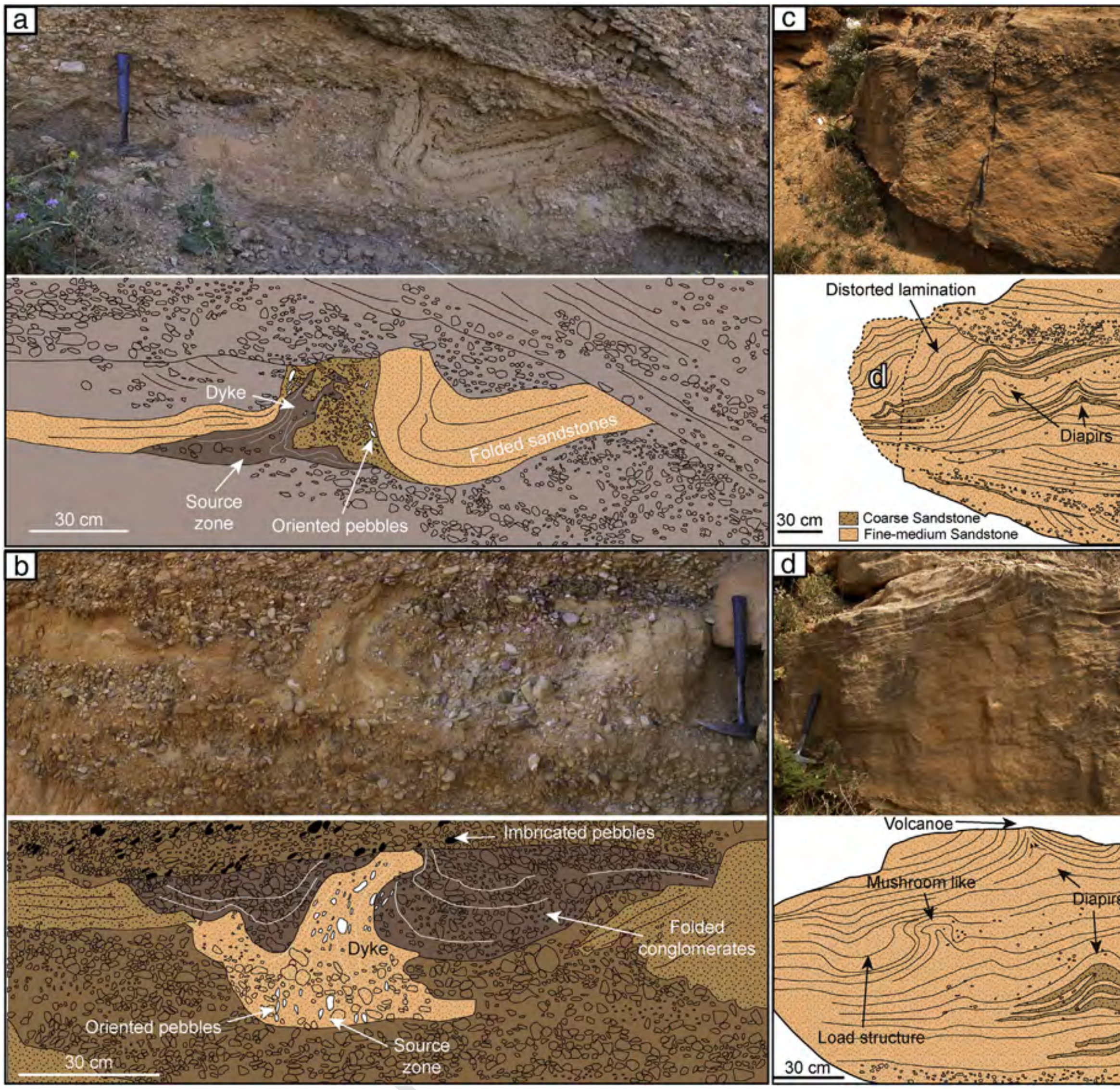

Fig. 9. (a) Large clastic dyke: single vertical conduit filled with fine-grained materials and crossing and deforming a sandstone bed. Source bed and oriented pebbles are shown. (b) Large clastic dyke: single vertical conduit filled with fine-grained materials and crossing and deforming the surrounding conglomerate. Source bed and oriented pebbles are shown. (c) Diapirs and load structures developed in a complete deformed sandstone channel body.

deposits of the Jiloca Basin can be interpreted as seismically-induced since it is possible to exclude the action of other trigger mechanisms. Some mechanisms that are able to induce liquefaction and fluidization are not compatible with the described facies associations such as wave action or sudden variations of the water-table depth. Furthermore, the palustrine-lacustrine facies described in the two studied well logs do not show evidence of storm-wave action, overloading or unequal loading processes. The only authigenic factor that could be invoked is overloading by gravel-dominated alluvial beds of Fig. 5 (Concud outcrops). Nevertheless, calculations and experimental analog models (Moretti et al., 2001) show that the height of deformation (h) in a substrate induced by the instantaneous deposition of a bed is more or less similar to its thickness (H). In our field examples, the overlying sediments are always well-laminated sands and gravels with imbrication, indicating deposition from tractive flows and excluding the possibility of rapid mass flows and its overloading effects. We also interpret the described slumps as seismites since they occur in almost-flat environments and in the absence of transient slopes associated with large-scale traction bedforms (Field et al., 1982; Spalluto et al., 2007; García-Tortosa et al., 2011; Mastrogiacomo et al., 2012; Alsop and Marco, 2013).

6.3. Lateral and vertical distribution of SSDSs

Once described and interpreted, the SSDSs recognized in the Ramblillas and Concud profiles can be combined with the results from Masada Cociero (Ezquerro et al., 2015) in order to analyze their overall distribution in the studied area. Fig. 6 shows, for each studied profile, their location and type of SSDSs, as well as the interpreted (seismic or non-seismic) origin.

The Masada Cociero profile contains most of the SSDSs recognized. Almost systematically, 1 or 2 non-seismic structures appear within each sub-unit in this profile, independently of the involved lithology. An exception is recognized in the evaporite facies of the two lower, I and II sub-units, where mudcrack levels are concentrated. Seismically induced SSDSs are also present in every sub-unit (usually, 2 or 3 structures). Nevertheless, a group that involves 12 structures developed in heterolitic facies is easily recognizable in sub-units III and IV.

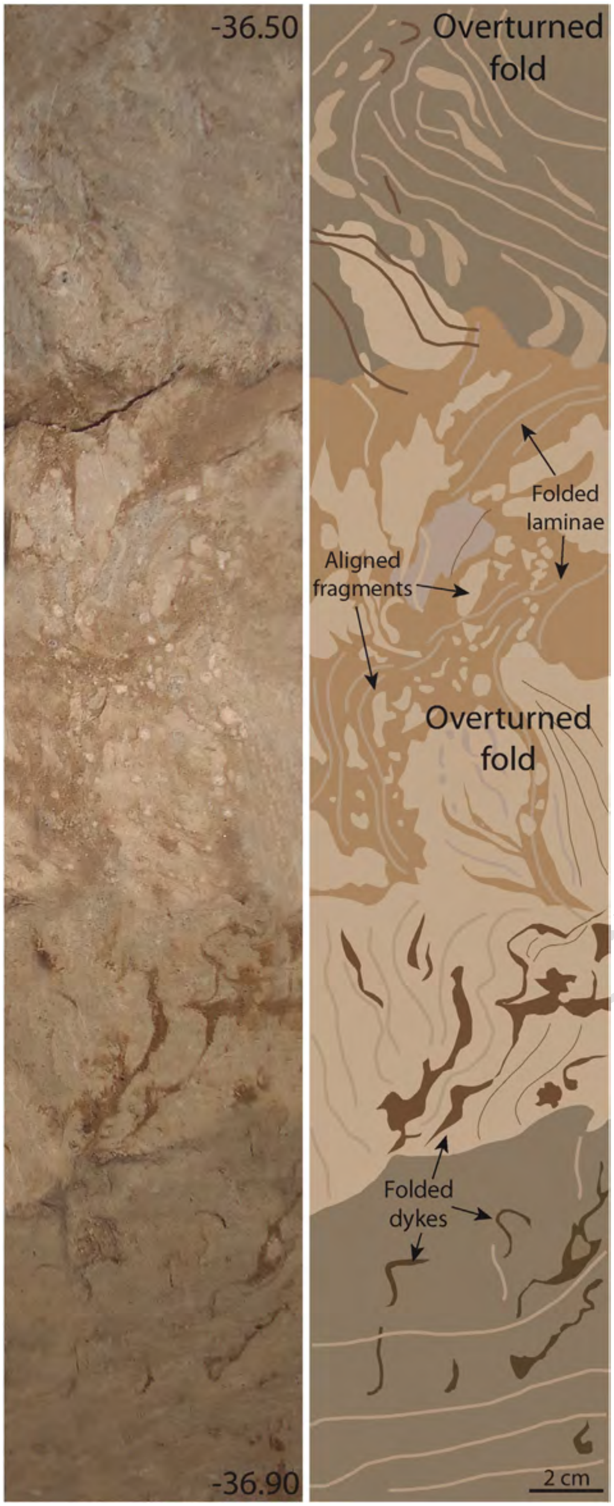

Fig. 10. The thickest slump sheet in the Ramblillas well core. Overturned folds deform white, grayish and brown carbonate silts laminae.

In the Ramblillas profile, non-seismic SSDSs show a similar vertical distribution that in Masada Cociero, with 1 or 2 deformation levels per sub-unit. However, seismically induced structures have been only recognized in the lower sub-units (II, III and IV sub-units), with a cluster of 10 seismically-induced beds in laminated silty facies of sub-units II and III.

The Concud profile, which was totally logged at outcrop and exhibits the most massive sediments, has the minimum number of recognized SSDSs. Non-seismic deformations correspond exclusively to bioturbation traces (1 or 2 structures per sub-unit) that were able to produce extensive distortion of deposits. The only 3 seismically induced SSDSs recognized are clustered within a clastic alternation at the top of the profile (sub-unit VII, *Villafranchian pediment* unit).

In the Concud-Teruel Residual Basin, most types of aseismic deformation structures appear *quasi* equally vertical spaced in the three studied sections and affect any sedimentary facies. According to our correlation model, they appear at similar stratigraphical positions, suggesting their lateral continuity. By contrast, seismites have a more irregular vertical distribution in different sections. Their lateral correlation is generally difficult where they appear isolated, while this becomes easier for seismite clusters (especially in sub-unit III of Masada Cociero and Ramblillas profiles). In sub-unit VII, lateral overlapping between the SSDSs groups of Concud and Masada Cociero profiles can be recognized. For sub-units I, V and VI, seismites only appear in the Masada Cociero profile.

After achieving the overall correlation of SSDS levels, a number between 29 and 35 seismic deformed levels have been computed for the whole stratigraphic section. For 6 deformation levels, we admit a seismic origin, but not undeniable correspondence between profiles. Such an inventory of seismites represents a valued paleosesimic archive for the time interval (between ~3.6 and ~1.9 Ma).

7. Discussion

7.1. Spatial and temporal occurrence of seismic and non-seismic SSDSs

The distribution of observed seismically-induced SSDSs is strongly heterogeneous along the different borehole and surface records (Figs. 3, 6): they occur along the whole well log at Masada Cociero, are concentrated at the lower part of the Ramblillas well log, and are virtually absent in surface profiles except for the uppermost part of the Concud profile.

As a first approach, the overall frequency of seismites decreases from profile 1 (Masada Cociero) to 2 (Ramblillas) and 3 (Concud), as the distance from the Concud Fault increases, which is consistent with a simple attenuation law from the fault that constitutes the main seismogenic source in the area. This evinces that the magnitude threshold commonly proposed for occurrence of seismic SSDSs (Mw ~ 5) is meaningful only for the epicentral area. Even though this magnitude could have been exceeded, the probability of seismite occurrence would diminish as the epicentral distance increases.

On the other hand, we should not forget that SSDSs distribution is also controlled by the observation scale and involved sedimentary facies (e.g., Alfaro et al., 1997; Rodríguez-López et al., 2007; Liesa et al., 2016), which can explain the scarcity of SSDSs in the westernmost, Concud profile. Outcropping conditions seem to have inhibited the recognition of SSDSs under decametric-scale, so that only a few, large SSDSs could be observed in this profile. Data from Concud correspond to more proximal, alluvial facies, showing predominance of massive, coarse clastic sediments, with low lithological variety and arranged in thicker beds. This makes it more difficult to develop conserve and recognize SSDSs, in contrast with those of palustrine-lacustrine areas.

Nevertheless, other pieces of evidence support the tectonic control on SSDS distribution. The clear difference between both well logs at the central-upper part of the succession (abundant seismically-induced SSDSs in Masada Cociero, virtual absence in Ramblillas) clearly supports the idea that most seismic events that occurred during chrons C2An.2n and C2r produced SSDSs only within a distance of less than 1 km from the fault trace. Since this did not occur for events during the previous chron C2An.3n, we can

Please cite this article as: Ezquerro, L., et al., Controls on space–time distribution of soft-sediment deformation structures: Applying palaeomagnetic dating to approach the *apparent*..., Sedimentary Geology (2016), http://dx.doi.org/10.1016/j.sedgeo.2016.06.007

infer that the magnitude of paleoseisms within the period C2An.2n was greater than during C2An.3n. Afterwards, a number of large paleoseisms again occurred during C2r, which were recorded by large-scale SSDSs in deposits of the *Villafranchian pediment* unit in spite of its unfavorable lithology.

Through the overall stratigraphic succession, although broadly distributed (2–3 structures per sub-unit, in average), seismites appear clustered, mainly in sub-units III and IV in Masada Cociero and sub-units II and III in Ramblillas. Both groups coincide with heterolithic or laminated facies, which points again to a lithological control. But they are also linked to an episode of increased sedimentation rate (0.17 mm/a, Fig. 11), which suggests close relationship with accelerated tectonic subsidence, therefore increasing activity of the Concud Fault. We exclude the climatic control on the sedimentation rate changes due to the fact that the succession becomes thicker towards the fault. However, a period of high sedimentation rate, between 2.128 and 1.945 Ma (Fig. 11), shows very scarce occurrence of SSDSs. We interpret this in terms of poor observation conditions, since this time span is entirely represented by the upper, surficial part of the Masada Cociero profile and the observation gap below. A similar case has been described in the Early Cretaceous Villanueva de Huerva Fm. in the Iberian Basin (Soria et al., 2013), where the maximum development of slumping coincides with episodes of tectonically-induced high sedimentation rate (evinced by thicker cycles of lake expansion-retraction related to precession Milankovitch cycle).

With respect to non-seismic deformations, these show a quite distinct distribution pattern. They appear regularly spaced in the studied series and are associated with any sedimentary facies. Such features, as well as their lateral arrangement at similar stratigraphical positions, point to cyclically pedogenic, mechanical or biological triggers that induced authigenic processes in the basin. Such processes, and hence the vertical distribution, might be ultimately controlled by climatic cycles (e.g. De Wet et al., 1998; Luzón et al., 2002; Abels et al., 2009; Soria et al., 2013). An exception to the regular occurrence of non-seismic SSDSs is the cluster of mudcrack levels in evaporite facies (sub-units I and II) in the Masada Cociero profile. These mudcracks probably developed in frequent desiccation episodes in such a saline environment.

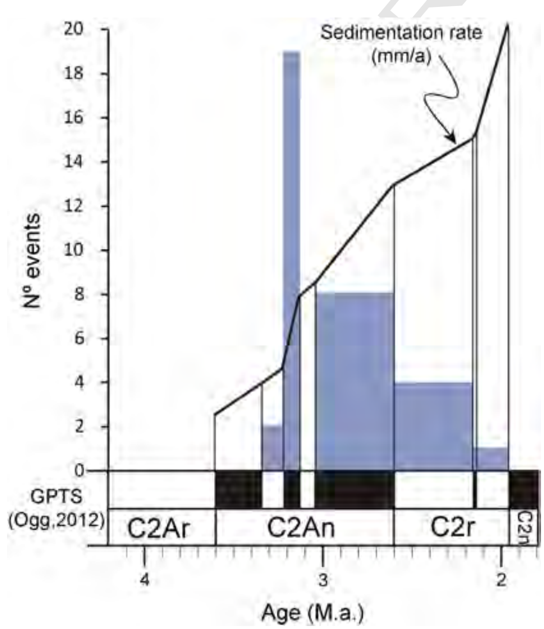

Fig. 11. Sedimentation rate vs. number of seismic events for each chron.

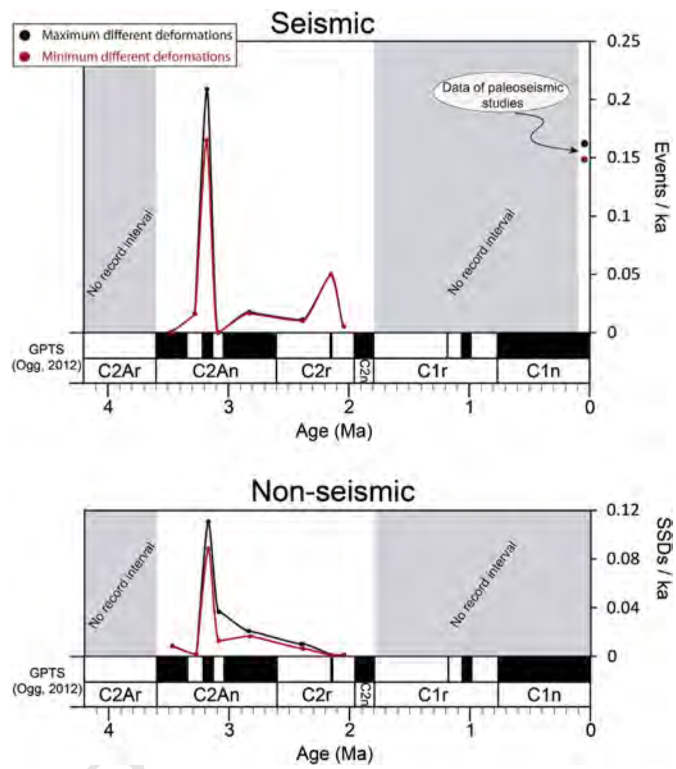

Fig. 12. Frequency (inverse of the *apparent recurrence period* in ka) of seismic events (M ≥ 5) and non-seismic SSDSs during the studied time interval.

7.2. Insights into the apparent recurrence period of paleoseisms and its time variation

After correlating every seismically-induced SSDSs level through the studied profiles, we have computed the total paleoseismic record and calculated the apparent frequency of paleoseismic events for each time slice represented by either a chron or a sub-chron (Fig. 12). Such frequency usually ranges from 0.01 to 0.02 events/ka, except for two periods (sub-chrons C2An.2n and C2r.1n), in which frequency increases up to 0.16 and 0.05, respectively, coinciding with (i) the high concentration of small-scale SSDSs in the lower part of both boreholes (paleoseisms that produced SSDSs within a distance exceeding 1 km), and (ii) large-scale SSDSs in coarse clastic sediments at the upper part of Concud (therefore, also representing relatively strong seisms).

Both periods with high paleoseismic frequency are quite short. One could suspect that such coincidence perhaps represents an artifact caused by biased sampling. Nevertheless, such SSDS ensembles represent sharp clusters in time but not in the thickness of the sedimentary succession. We have explained how both coincide with periods of high sedimentation rate; therefore, their correspondence with periods of high tectonic subsidence, and hence their tectonic control, is proved.

From results compiled in Fig. 12, we have computed the corresponding apparent recurrence periods (represented in the figure as frequency of seismicity). After computing 35 seismic events between ~3.6 and ~1.9 Ma, an average recurrence period of ~47 ka is calculated for the whole succession. This value is close to the first estimation by Ezquerro et al. (2015). The background value is between 56 and 108 ka, considering the maximum and minimum different SSDSs, while periods with high frequency of seismic pulses represent around to 4.8 to 6.1 ka.

7.3. Comparison with Pleistocene paleoseismicity

After calculating those *apparent recurrence periods* of paleoseisms for a number of time intervals within the Late Pliocene-Early Pleistocene, it seems pertinent to compare them with the recurrence times obtained from trench analysis in Late Pleistocene deposits of the same area to provide a wider temporal viewpoint for assessing the activity pattern of the Concud Fault.

Briefly, we have explained how the average recurrence period of large earthquakes (*characteristic earthquakes*) for the last 74 ka has been calculated at between 7.1 and 8.0 ka, based on identification of eleven paleoseismic events in five trenches along the Concud Fault (Lafuente et al., 2014; Simón et al., 2015). This range approaches the *apparent recurrence period* (4.8 to 6.1 ka) calculated for the time interval with the maximum frequency of seismic SSDSs. i.e. the sub-chron C2An.2n. It is noteworthy that the duration of this sub-chron (91 ka) is of the same order as the time span covered by trench studies (74 ka), which allows us to rule out any bias related to representativeness of the computed period.

Going deeper into this issue, we should remember that the threshold commonly proposed for occurrence of seismic SSDSs (Mw ~ 5) is remarkably lower than that inferred for the characteristic earthquake at the Concud Fault (Mw = 6.5–6.6), so that our apparent recurrence period from SSDSs is expectable to be shorter than the average recurrence period of the characteristic earthquake. The 500-year seism for this fault, calculated by interpolating between historic-instrumental and paleoseismic records, is M ~ 5.3 (Simón et al., 2014). Therefore, 0.5 ka would represent a more realistic value for the expectable recurrence period obtained from seismites.

Nevertheless, paleoearthquakes below the *characteristic magnitude* are likely not linked to activation of the entire Concud Fault surface. Therefore, they did not involve surface rupture, and their foci could be located quite far from our studied boreholes (up to ~20 km, according to the length and depth of the fault). In such a case, the studied boreholes would be out of the epicentral area, and we should not expect every seism of that magnitude to be recorded in them. In summary, our apparent recurrence period (4.8–6.1 ka), bracketed between the recurrence period corresponding to the SSDSs threshold magnitude (~ 0.5 ka) and that of the characteristic earthquake of the closest seismogenic fault (7.1–8.0 ka), can be considered as a consistent result.

After that successful comparison between their respective paleoseismic patterns, we can infer that both the Late Pleistocene (and Holocene?) and the sub-chron C2An.2n within the Late Pliocene (3.207–3.116 Ma) were periods of high activity along the Concud Fault history. The curve of sedimentation rate in Figs. 7, 11 provides a framework for assessing such temporal pattern of activity, since it can be interpreted as a proxy of variation of tectonic subsidence with time. Values of sedimentation rate for the Late Pliocene should be considered as slightly lower than those of tectonic subsidence: sedimentation is constrained to the Teruel-Concud Residual Basin, but sedimentological features of the infill do not evince any noticeable positive relief at its margins (Ezquerro et al., 2015). In this sense, the coincidence between both periods of high activity is also remarkable: the maximum sedimentation rate recorded in the Masada Cociero succession (0.17 mm/a) corresponds to the sub-chron C2An.2n and approaches the average slip rate (0.29 mm/a) calculated for the last 74 ka (Simón et al., 2015).

These periods of high activity would have alternated with periods of low activity (*apparent recurrence period* of seismic events in the range of 56 to 108 ka; sedimentation rate as low as 0.02 mm/a, see Figs. 7, 11), resulting in average values, for the overall studied time interval, of 47 ka and 0.06 mm/a, respectively. Such alternation, at a time scale of the order of 10^5 years, is modulated by a similar fluctuation at a more detailed scale (10^4 years), as shown by the slip history of the Concud Fault during the Late Pleistocene. The latter is characterized by alternating periods of faster slip (74.5 to 60 ka BP, 0.53 mm/a; 21 to ca. 8 ka BP, 0.42 mm/a) and slower slip (60 to 21 ka BP, 0.13 mm/a) (Lafuente et al., 2014; Simón et al., 2015). This suggests a *fractal* pattern in the occurrence of seismic events through time, with clusters that could be identified at every time scale, depending on the observation time window. Instrumental earthquake swarms would be the shortest and most recent example of such seismic clusters indeed.

From the methodological point of view, we should notice the coincidence of time occurrence patterns recognized for peaks of paleosesimic activity in the studied area from both primary evidence in trenches and secondary evidence in boreholes. This gives support to the notion of the *apparent recurrence period* as defined by Ezquerro et al. (2015). At least for those calculated from SSDS inventories collected in borehole logs close to seismogenic faults, *apparent recurrence periods* are comparable to actual recurrence times of paleoearthquakes (those exceeding the SSDSs magnitude threshold and approaching the *characteristic* magnitude).

8. Conclusions

A high number of SSDSs (35 of seismic origin and 28 of non-seismic origin) have been identified in three sections (Concud, Ramblillas and Masada Cociero), logged from boreholes and outcrops in Late Pliocene-Early Pleistocene deposits of the Teruel-Concud Residual Basin, close to the Concud normal fault. They belong to a variety of types, such as clastic dykes, load structures, diapirs, slumps, nodulizations or mudcracks.

Timing of seismic and non-seismic SSDSs has been initially constrained from biostratigraphic data (mammal sites) and a previous magnetostratigraphic profile (Opdyke et al., 1997), then substantially refined from a new magnetostratigraphic study at Masada Cociero site. The overall stratigraphic section and the recorded SSDSs cover a time span between ~3.6 and ~1.9 Ma.

Non-seismic SSDSs are relatively well-correlated between sections, while seismic ones are poorly correlated, except for several clusters of structures. After achieving the correlation, a number between 29 and 35 seismically deformed levels have been computed for the overall stratigraphic section.

Main controls on the lateral and vertical distribution of the SSDSs are: i) origin (either seismic or non-seismic) of deformation structures; ii) distance to seismogenic source (the Concud Fault); and iii) sedimentary facies involved in deformation.

The paleoseismites are broadly distributed along the Upper Pliocene-Lower Pleistocene Teruel-Concud Residual Basin, but their record is more complete near the Concud Fault, i.e. near the source for paleoseisms and where the sedimentary facies, ultimately controlled by tectonic subsidence, was also more suitable for their development.

In the overall stratigraphic section (~3.6 to ~1.9 Ma), seismites show an apparent recurrence period of 56–108 ka. Clustering of eighteen seismic SSDSs levels within the chron C2An.2n (3.207 to 3.116 Ma) reveals much higher paleoseismic activity, with an apparent recurrence period of 4.8 to 6.1 ka. Increase in sedimentation rate, and hence tectonic subsidence, during this interval reinforces the scenario of SSDSs triggered by the Concud Fault activity.

The Late Pliocene-Early Pleistocene activity of the Concud Fault shows a similar behavior to that for the Late Pleistocene (last ca. 74 ka BP), with alternating periods of faster and slower slip. The difference is the time scale of the recognized fluctuations: of the order of 10^5 years for the Late Pliocene-Early Pleistocene, and 10^4 years for the Late Pleistocene.

In the study area, time occurrence patterns recognized for peaks of paleosesimic activity from secondary evidence in boreholes are similar to those inferred from primary evidence in trenches. This gives support to the notion of *apparent recurrence period* as defined by Ezquerro et al. (2015). At least for those calculated from SSDS inventories collected in

Please cite this article as: Ezquerro, L., et al., Controls on space–time distribution of soft-sediment deformation structures: Applying palaeomagnetic dating to approach the *apparent*..., Sedimentary Geology (2016), http://dx.doi.org/10.1016/j.sedgeo.2016.06.007

borehole logs close to the seismogenic faults, *apparent recurrence periods* are comparable to actual recurrence times of large paleoearthquakes.

Uncited reference

Alfaro et al., 1995

Acknowledgments

We would thank J.J. Díaz-Martínez and G. Owen for their valuable comments and suggestions which have permitted to improve the final version of our manuscript. Special thanks to Cristina García-Lasanta for helping us during the paleomagnetic fieldwork and Elisa Sanchez and the laboratory of the University of Burgos. Research has been supported by project CGL2012-35662 of the Spanish Ministerio de Economía y Competitividad-FEDER, as well as by the Aragón regional government ("Geotransfer" and "Análisis de Cuencas Sedimentarias Continentales" research groups). L. Ezquerro benefited from a FPI grant (BES-2010-031339) of Spanish Ministerio de Economía y Competitividad.

Appendix A. Paleomagnetism

A.1. Sampling and laboratory procedures

Paleomagnetic sampling (one sample each 0.5 m, except in the sedimentary gaps) was performed using both, standard drilling techniques and soft material extraction procedures. In total, 160 standard paleomagnetic cores were obtained; 26 samples come for the Masada Cociero outcrop and 134 samples were taken in the well core obtained with an extractor of soft materials. Samples were consolidated later in the laboratories of the University of Zaragoza using Sodium silicate (50% solution) and Aluminum cement (Pueyo et al., 2006).

Every standard sample gave 1–2 specimens and 263 of them were demagnetized in the laboratory (≈ 2 specimens per stratigraphic level in average out). Paleomagnetic measurements were taken at the laboratory of the Applied Physics Department of the University of Burgos (Spain). Stepwise thermal demagnetization was successfully applied to separate magnetic components in most samples. Different routines were used; steps every 50 °C at low temperatures (only until 400–550 °C) and every 20°-30 °C at the higher ones or, alternatively, increments of 50 °C up to 450 °C; increments of 25 °C up to 575 °C and 20 °C steps until the end (680 °C). Demagnetization routine was always designed to reach high temperatures by means of 18 steps. Measurements were done using a 2G superconducting cryogenic magnetometer and MMTD80A (by Magnetic Measurements Ltd) and TD-48 (by ASC Scientific Ltd) ovens.

Directions of the Characteristic remanent magnetization (ChRM) were fitted using the software VPD (Ramón and Pueyo, 2012 and Ramón, 2013) that allows the standard principal component analysis (Kirschvink, 1980) and the demagnetization circles technique (Bailey and Halls, 1984). Fisher (1953) statistics was applied to obtain spherical means using the stereonet program (Allmendinger et al., 2012).

A.2. Paleomagnetic stability

Isothermal remanent magnetization (IRM) acquisition curves outline the contribution of different magnetic mineral to the remanence, in relation to the lithological variety. The thermal demagnetization of the 3-componets IRM (Lowrie's test, 1990) has helped us to characterize the different carriers of the magnetization. In carbonate, evaporate and withish rocks, magnetically soft mineralogy is predominant and is saturated at low magnetic fields. Hard mineralogy represented by phases of high coercivity cannot fully ruled out but it displays a minor contribution in these samples (Fig. Appendix 1). In reddish mudstones and sandstones, the dominant contribution to the remanence is imposed by the hard mineralogy, mostly hematite. A frequent decay at 300 °C has also been observed attesting for the presence of iron sulfides in many lithologies, especially in organic rich levels and siltstones with high levels of organic matter. Many of the samples showing iron sulfides also shown remanences unblocking up to 550 to 600 °C. Red mudstones and sandstones unblock at higher temperature > 600 °C (Fig. 5). All these results point to magnetite as the main carrier of the remanence in the Masada Cociero, although iron sulfurs and hematite contributing to the remanence in some cases.

A.3. Re-orientation methodology

The samples coming from the well core have been extracted perpendicular to an arbitrary orientation line which is parallel to the well core axis, besides top and base of the section is known. Thus, each sample is perpendicular to the well core axis. In this way, a common reference system for all specimens is established, allowing for a direct comparison of their paleomagnetic data (Bleakly et al., 1985; Van Alstine et al., 1991; Van Alstine and Butterworth, 1993; Hamilton et al., 1995).

VRM has a declination −0.2829° W and an inclination 55.1873° using the field model WMM2015 (www.ngdc.noaa.gov) in the Concud location (latitude: 40.30° N, longitude: 1.15° W; elevation: 1.0 km over the mean sea level). The viscous component of most samples (Fig. Appendix 2) shows inclination values almost coincident to the expected present-day geomagnetic field (deduced from the NOAA's National Geophysical Data Center using the IGRF12-gufm1 model (Jackson et al., 2000), although the drilling orientation induces a slightly modification in the NRM and VRM orientations respect to the present day field (Fig. Appendix 3). Thus reorientation method can be applied.

Once the amount of rotation between the initial direction and the true direction of the VRM is known, the ChRM have been jointly rotated to its probable orientation, giving the true orientation of the sample. Re-oriented magnetic data are approximately antipodal directions of normal polarity (upper hemisphere) with respect to reverse polarity (lower hemisphere); 348, 75 ($\alpha 95$: 6.7°; k: 4.7 and R: 0.7866) and 145, −81 ($\alpha 95$: 127°, k: 3.0 and R: 0.6773), which share a common true mean (Fig. Appendix 2). Besides, the combined mean vector in the lower hemisphere (173, 75; $\alpha 95$: 6.8°, k: 4.6 and R: 0.7866) falls very close to the expected Plio-Pleistocene reference direction (Dec: 002, Inc.: 65). This reference was deduced for the Masada Cociero location (Latitude: 55° 9′ 50′ 'N, Longitude: 0° 48′ 5″ W) using the Plio-Pleistocene poles of Iberia (Osete and Palencia, 2006).

A.4. Quality filter

Samples from different classes are in similar proportions: 30% samples are class I, 40% samples class II and class III approximately represents a 30% of the dataset. Focusing only on directions used for building the LPS (classes I and II); ≈ 86% of them display MAD <20° and are characterized by more than 5 demagnetization steps in average (Fig. Appendix 4). Focusing only on directions used for building the LPS (classes I and II); ≈ 86% of them display MAD <20° and are characterized by more than 5 demagnetization steps in average. Some additional criteria were set up to define a magnetozone: i) two or more consecutive stratigraphic levels with the same polarity sign (VGP); ii) at least one level (usually more) must belong to the class I group; and iii) following the concept by Vandamme (1994) and Deenen et al. (2011), a ± 30° cutoff for the VGP latitude around the equator helps removing undesirable noise.

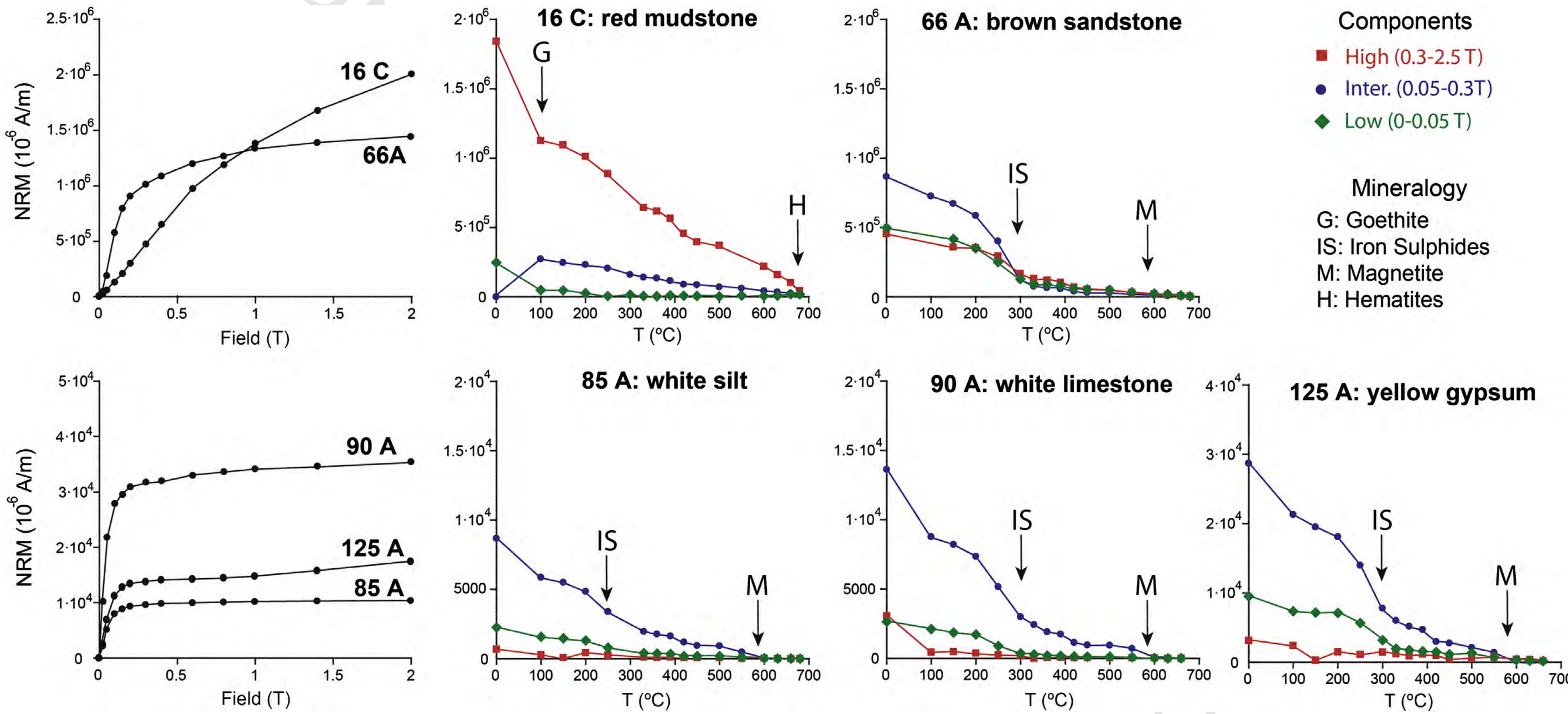

Appendix Fig. 1. IRM acquisition curves and thermal demagnetization results of a three-component IRM of representative lithologies samples. G, IS, M and H indicates the decay of remanence associated with Goethite, Iron Sulfides, Magnetite and Hematite, respectively.

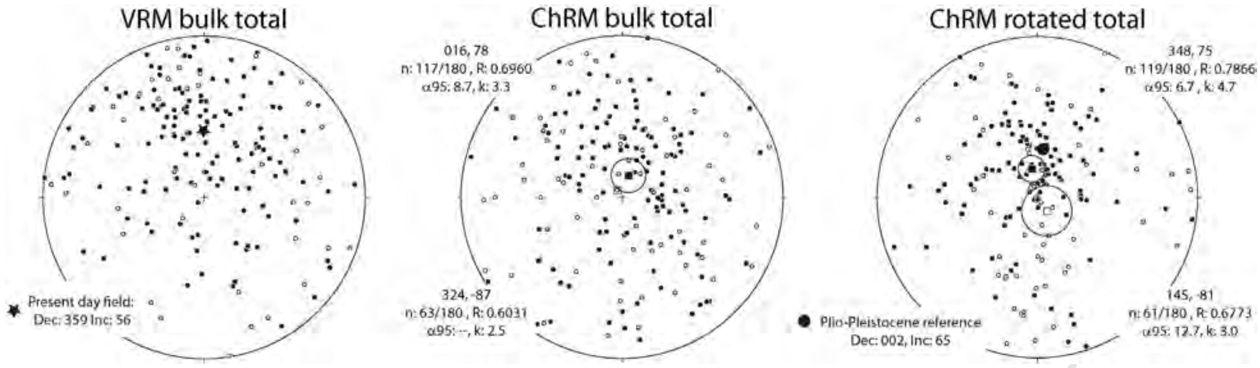

Appendix Fig. 2. Characteristic directions from the Masada Cociero section in the stereonet. Only class I and II samples were used in these plots. VRM inclination is relatively closed to the Q12 present day field. VRM and ChRM data display an arbitrary distribution; ChRM after paleogeographic correction shows antipodality. Fisher (1953) means are also displayed.

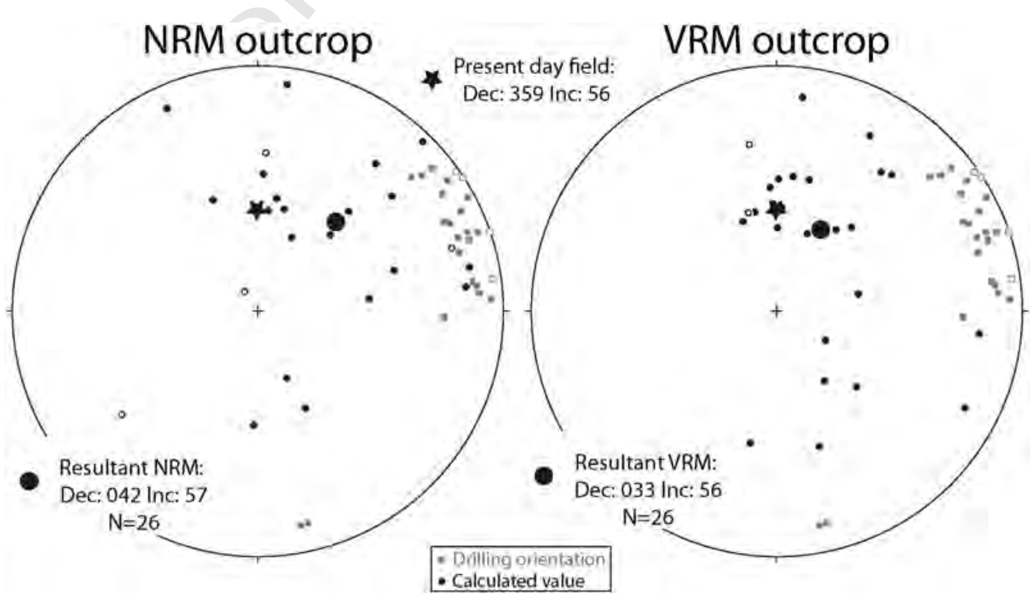

Appendix Fig. 3. Drilling modifies the NRM and VRM orientations. Black symbols represent the NRM and VRM resultant of the samples and gray symbols imply the drilling orientation.

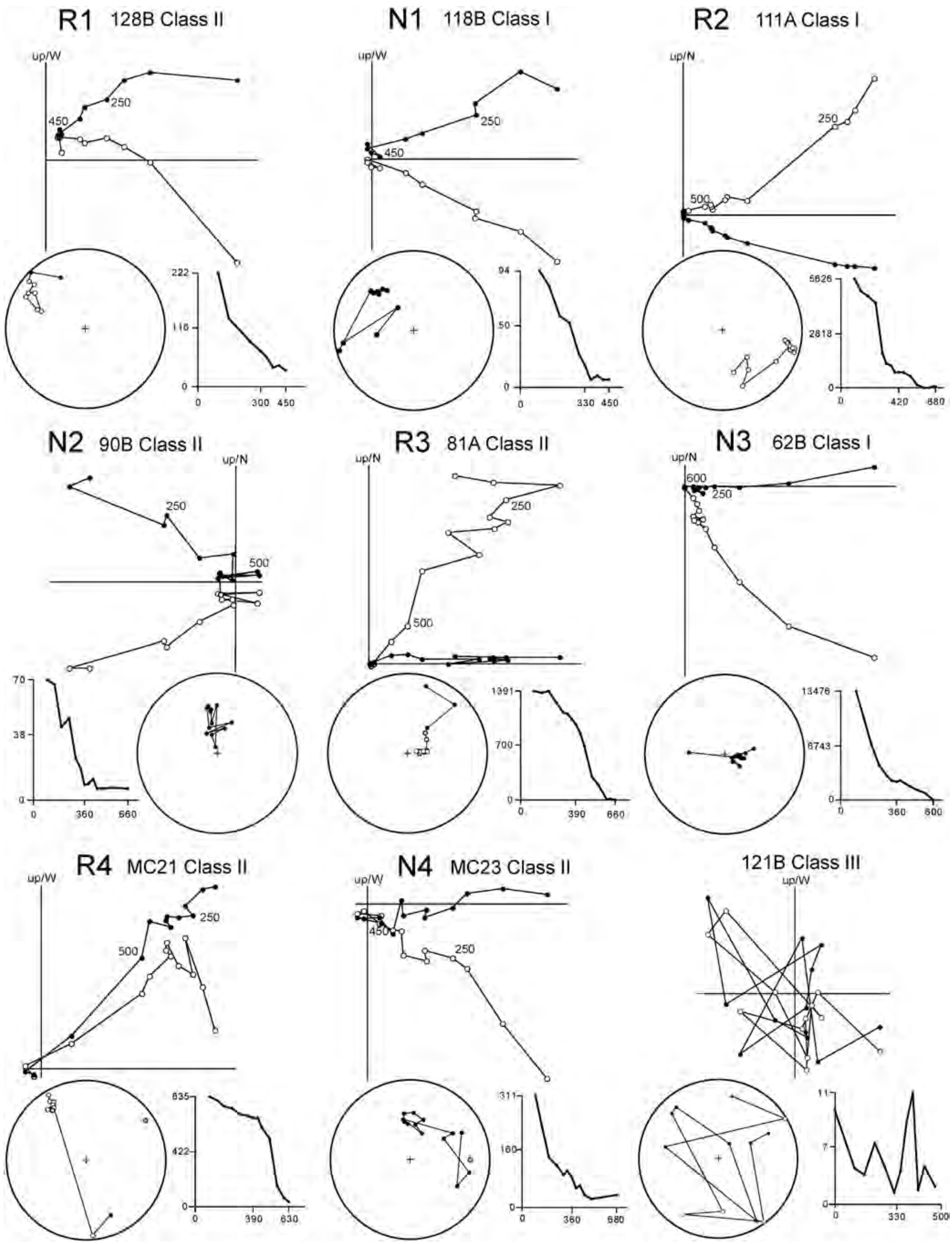

Appendix Fig. 4. Thermal stepwise demagnetization of the NRM; orthogonal diagrams from the Masada Cociero section. Displayed samples are evenly distributed along the studied profiles (local magnetozone number is shown for every diagram). Intensity decay curves in 10–6 A/m and stereographic projections. Gray circle in the stereonets represent the orientation of drilling. Diagrams derived from the VPD program (Ramón, 2013).

References

Abels, H.A., Abdul Aziz, H., Ventra, D., Hilgen, F.J., 2009. Orbital climate forcing in mudflat to marginal lacustrine deposits in the Miocene Teruel Basin (Northeast Spain). Journal of Sedimentary Research 79, 831–847.

Adrover, R., 1986. Nuevas Faunas De Roedores en El Mioplioceno Continental de la región de Teruel (España). Interés biostratigráfico Y paleoecológico. Instituto de Estudios Turolenses, Teruel (433 pp.).

Adrover, R., Mein, P., Moissenet, E., 1978. Nuevos datos sobre la edad de las formaciones continentales neogenas de los alrededores de Teruel. Estudios Geológicos 34, 205–214.

Alcalá, L., Alonso-Zarza, A.M., Álvarez, M.A., Azanza, B., Calvo, J.P., Cañaveras, J.C., van Dam, J.A., Garcés, M., Krijgsman, W., van der Meulen, A.J., Morales, J., Peláez, P., Pérez-González, A., Sánchez, S., Sancho, R., Sanz, E., 2000. El Registro sedimentario y faunístico de las cuencas de Calatayud-Daroca y Teruel. Evolución paleoambiental y paleoclimática durante el Neógeno. Revista de la Sociedad Geológica de España 13, 323–343.

Alfaro, P., Domènech, C., Estévez, A., Soria, J.M., 1995. Estructuras de deformación en sedimentos del Cuaternario reciente de la Cuenca del bajo Segura (Alicante). Discusión sobre su posible origen sísmico. Geogaceta 17, 91–94.

Alfaro, P., Moretti, M., Soria, J.M., 1997. Soft-sediment deformation structures induced by earthquakes (seismites) in Pliocene lacustrine deposits (Guadix-Baza Basin, central Betic cordillera). Eclogae Geologicae Helvetiae 90, 531–540.

Alfaro, P., Gibert, L., Moretti, M., García-Tortosa, F.J., Sanz de Galdeano, C., Galindo-Zaldívar, J., López-Garrido, T.C., 2010. The significance of giant seismites in the plio–Pleistocene Baza palaeo-lake (S Spain). Terra Nova 22, 172–179.

Allen, J.R.L., 1986. Earthquake magnitude-frequency, epicentral distance, and soft-sediment deformation in sedimentary basins. Sedimentary Geology 46, 67–75.

Allmendinger, R.W., Cardozo, N., Fisher, D., 2012. Structural Geology Algorithms: Vectors and Tensors in Structural Geology. Cambridge University Press.

Alonso-Zarza, A.M., Calvo, J.P., 2000. Palustrine sedimentation in an episodically subsiding basin: the Miocene of the northern Teruel graben (Spain). Palaeogeography, Palaeoclimatology, Palaeoecology 160, 1–21.

Alonso-Zarza, A.M., Meléndez, A., Martín-García, R., Herrero, M.J., Martín-Pérez, A., 2012. Discriminating between tectonism and climate signatures in palustrine deposits: 2 lessons from the Miocene of the Teruel graben, NE Spain. Earth-Science Reviews 113 (3), 141–160.

Alsop, G.I., Marco, S., 2013. Seismogenic slump folds formed by gravity-driven tectonics down a negligible subaqueous slope. Tectonophysics 605, 48–69.

Álvaro, M., Capote, R., Vegas, R., 1979. Un Modelo de evolución geotectónica Para la Cadena Celtibérica. Acta Geologica Hispánica 14, 172–177.

Bailey, R.C., Halls, H.C., 1984. Estimate of confidence in paleomagnetic directions derived from mixed magnetization circle and direct observational data. Journal of Geophysics 54, 174–182.

Bleakly, D.C., Van Alstine, D.R., Packer, D.R., 1985. Core orientation 1: controlling errors minimizes risk and cost in core orientation. Oil and Gas Journal 83 (48), 103–109.

Capote, R., Muñoz, J.A., Simón, J.L., Liesa, C.L., Arlegui, L.E., 2002. Alpine Tectonics I: the Alpine System north of the Betic Cordillera. In: Gibbons, W., Moreno, T. (Eds.), Geology of Spain. Geological Society of London, London, pp. 367–400.

Davenport, C.A., Ringrose, P.S., 1987. Deformation of Scottish Quternary Sediment Sequences by Strong Earthquake Motions. In: Jones, M.E., Preston, R.M.F. (Eds.), Deformation of Sediments and Sedimentary Rocks. The Geological Society, London, Special Publication 29, pp. 299–314.

De Wet, C., Yocum, D.A., Mora, C., 1998. Carbonate lakes in closed basins: sensitive indicators of climate and tectonics: an example from the Gettysburg Basin (Triassic), Pennsylvania, USA. Role of Eustasy, climate and tectonism in continental rocks. SEPM Special Publication 59, 191–209.

Deenen, M.H.L., Langereis, C.G., van Hinsbergen, D.J.J., Biggin, A.J., 2011. Geomagnetic secular variation and the statistics of palaeomagnetic directions. Geophysical Journal International 186 (2), 509–520.

Dzulynski, S., Walton, E.K., 1965. Sedimentary Features of Flysch and Greywackes. Developments in Sedimentology 7. Elsevier, Amsterdam.

Eissmann, L., 1994. Grundzüge der Quartärgeologie Mitteldeutschlands (Sachsen, Sachsen-Anhalt, Südbrandenburg, Thüringen). Altenburger Naturwissenschaftliche Forschung 7, 55–135.

El Taki, H., Pratt, B.R., 2012. Syndepositional tectonic activity in an epicontinental basin revealed by deformation of subaqueous carbonate laminites and evaporites: seismites in Red River strata (upper Ordovician) of southern Saskatchewan, Canada. Bulletin of Canadian Petroleum Geology 60 (1), 37–58.

Ezquerro, L., Luzón, M.A., Liesa, C.L., Simón, J.L., 2012a. Evolución Megasecuencial del Relleno Mio-Plioceno del Sector Norte de la Cuenca de Teruel: Interacciones Entre tectónica Y sedimentación. In: Fernández, L.P., Fernández, A., Cuesta, A., Bahamonde, J.R. (Eds.), GeoTemas 13. Resúmenes Extendidos Del VIII Congreso Geológico de España, Oviedo, pp. 171–174.

Ezquerro, L., Lafuente, P., Pesquero, M.D., Alcalá, L., Arlegui, L.E., Liesa, C.L., Luque, L., Rodríguez-Pascua, M.A., Simón, J.L., 2012b. Una cubeta endorreica residual plio-pleistocena en la zona de relevo entre las fallas de Concud y Teruel: implicaciones paleogeográficas. Revista de la Sociedad Geológica de España 25, 157–175.

Ezquerro, L., Luzón, A., Navarro, M., Liesa, C.L., Simón, J.L., 2014a. Climatic vs. tectonic signal in the Neogene extensional Teruel basin (NE Spain), based on stable isotope (δ18O) and megasequential evolution. Terranova 26 (5), 337–346.

Ezquerro, L., Liesa, C.L., Simón, J.L., Arlegui, L.E., Luzón, A., Lafuente, P., 2014b. Correlation of sedimentary units from grain-size and mineralogic analyses as a tool for constraining trench interpretation in paleoseismology. International Journal of Earth Sciences 103 (8), 2327–2333.

Ezquerro, L., Moretti, M., Liesa, C.L., Luzón, A., Simón, J.L., 2015. Seismites from a well core of palustrine deposits as a tool for reconstructing the palaeoseismic history of a fault. Tectonophysics 655, 191–205.

Field, M.E., Gardner, V., Jennings, A.E., Edwards, B.D., 1982. Earthquake-induced sediment failures on a 0.25° slope, Klamath River delta, California. Geology 10, 542–546.

Fisher, R.A., 1953. Dispersion on a sphere. Proceedings of the Royal Astronomical Society 217, 295–305.

Fuller, M., 1969. Magnetic orientation of borehole cores. Geophysics 34, 772–774.

Garcés, M., Krijgsman, W., Van Dam, J., Calvo, J.P., Alcalá, L., Alonso-Zarza, A.M., 1999. Late Miocene alluvial sediments from the Teruel area: magnetostratigraphy, magnetic susceptibility, and facies organization. Acta Geologica Hispánica 32, 171–184.

García-Tortosa, F.J., Alfaro, P., Gibert, L., Scott, G., 2011. Seismically induced slump on an extremely gentle slope (<1 degrees) of the Pleistocene Tecopa paleolake (California). Geology 39 (11), 1055–1058.

Gibert, L., Alfaro, P., García-Tortosa, F.J., Scott, G., 2011. Superposed deformed beds produced by single earthquakes (Tecopa Basin, California): insights into paleoseismology. Sedimentary Geology 235 (3–4), 148–159.

Godoy, A., Ramírez, J.I., Olivé, A., Moissenet, E., Aznar, J.M., Aragonés, E., Aguilar, M.J., Ramírez del Pozo, J., Leal, M.C., Jerez-Mir, L., Adrover, R., Goy, A., Comas, M.J., Alberdi, M.T., Giner, J., Gutiérrez-Elorza, M., Portero, J.M., Gabaldón, V., 1983a. Hoja geológica núm. 567 (Teruel). Mapa Geológico de España E. 1:50.000. IGME, Madrid.

Godoy, A., Olivé, A., Moissenet, E., 1983b. Hoja geológica núm. 542 (Alfambra). Mapa Geológico de España E. 1:50.000. IGME, Madrid.

Guiraud, M., Plaziat, J.-C., 1993. Seismites in the fluviatile Bima sandstones: identification of paleoseisms and discussion of their magnitudes in a cretaceous synsedimentary strike-slip basin (upper Benue, Nigeria). Tectonophysics 225, 493–522.

Gutiérrez, F., Gutiérrez, M., Gracia, F.J., McCalpin, J.P., Lucha, P., Guerrero, J., 2008. Plio-quaternary extensional seismotectonics and drainage network development in the central sector of the Iberian range (NE Spain). Geomorphology 102, 21–42.

Hailwood, E.A., Ding, F., 1995. Palaeomagnetic Reorientation of Cores and the Magnetic Fabric of Hydrocrabon Reservoir Sands. In: Turner, P., Turner, A. (Eds.), Palaeomagnetic Applications in Hydrocarbon, Exploration and Production. Geological Society Special Publication 98, pp. 245–258.

Hamilton, W.D., Van Alstine, D.R., Butterworth, J.E., Raham, G., 1995. Paleomagnetic Orientation of Fractures in Jean Marie Member Cores from NE British Columbia/NW Alberta. The Petroleum Society of CIM, pp. 56–95.

Jackson, A., Jonkers, A.R.T., Walker, M.R., 2000. Four centuries of geomagnetic secular variation from historical records. Philosophical Transactions of the Royal Society of London 358, 957–990.

Kirschvink, J.L., 1980. The least-squares line and plane and the analysis of paleomagnetic data. Geophysical Journal of the Royal Astronomical Society 62, 699–718.

Krijgsman, W., 1996. Miocene magnetostratigraphy and cyclostratigraphy in the Mediterranean: extension of the astronomical polarity time scale. Geologica Ultraiectina 141, 1–207.

Krijgsman, W., Garcés, M., Langereis, C.G., Daams, R., van Dam, J., van der Meulen, A.J., Agustí, J., Cabrera, L., 1996. A new chronology for the middle to late Miocene continental record in Spain. Earth and Planetary Science Letters 142, 367–380.

Lafuente, P., 2011. Tectónica Activa Y Paleosismicidad de la Falla de Concud (Cordillera Ibérica Central) PhD Thesis Universidad de Zaragoza, Zaragoza.

Lafuente, P., Arlegui, L.E., Liesa, C.L., Simón, J.L., 2011a. Paleoseismological analysis of an intraplate extensional structure: the Concud fault (Iberian chain, Spain). International Journal of Earth Sciences 100, 1713–1732.

Lafuente, P., Arlegui, L.E., Casado, I., Ezquerro, L., Liesa, C.L., Pueyo, Ó., Simón, J.L., 2011b. Geometría y cinemática de la zona de relevo entre las fallas neógeno-cuaternarias de Concud y Teruel (cordillera Ibérica). Revista de la Sociedad Geológica de España 24, 117–132.

Lafuente, P., Arlegui, L.E., Liesa, C.L., Pueyo, Ó., Simón, J.L., 2014. Spatial and temporal variation of paleoseismic activity at an intraplate, historically quiescent structure: the Concud fault (Iberian chain, Spain). Tectonophysics. http://dx.doi.org/10.1016/j.tecto.2014.06.012.

Liesa, C.L., Rodríguez-López, J.P., Ezquerro, L., Alfaro, P., Rodríguez-Pascua, M.A., Lafuente, P., Arlegui, L., Simón, J.L., 2016. Facies control on seismites in an alluvial–aeolian system: the Pliocene dunefield of the Teruel half-graben basin (eastern Spain). Sedimentary Geology. http://dx.doi.org/10.1016/j.sedgeo.2016.05.009.

Lowe, D.R., 1975. Water escape structures in coarse-grained sediments. Sedimentology 22, 157–204.

Lowrie, W., 1990. Identification of ferromagnetic minerals in a rock by coercivity and unblocking temperature properties. Geophysical Research Letters 135, 159–162.

Luzón, A., González, A., Muñoz, A., Sánchez-Valverde, B., 2002. Upper Oligocene–lower Miocene shallowing-upward lacustrine sequences controlled by periodic and non-periodic processes (Ebro Basin, northeastern Spain). Journal of Paleolimnology 28, 441–456.

Mastrogiacomo, G., Moretti, M., Owen, G., Spalluto, L., 2012. Tectonic triggering of slump sheets in the upper cretaceous carbonate succession of the Porto Selvaggio area (Salento peninsula, southern Italy): synsedimentary tectonics in the Apulian carbonate platform. Sedimentary Geology 269–270, 15–27.

Mein, P., 1975. Resultats Du Groupe de Travail Des Vertebres. Report on Activity of the R.C.M.N.S. Working Groups, Bratislava, pp. 77–81.

Mein, P., Moissenet, E., Adrover, R., 1983. L'extension et l'ige des formations continentales pliocenes du fossé de Teruel. Comptes Rendus de l'Academie des Sciences de Paris 296, 1603–1610.

Mein, P., Moissenet, E., Adrover, R., 1990. Biostratigraphie du Neogene superieur de Teruel. Paleontología i Evolució 23, 121–139.

Migowski, C., Agnon, A., Bookman, R., Negendank, J.F.W., Stein, M., 2004. Recurrence pattern of Holocene earthquakes along the Dead Sea transform revealed by varvecounting and radiocarbon dating of lacustrine sediments. Earth and Planetary Science Letters 222, 301–314.

Moissenet, E., 1980. Relief et deformations récentes trois transversales dans les fossés internes des chaînes Ibériques orientales. Revue de Géographie des Pyrenées Sud-Ouest 51, 315–344.

Moissenet, E., 1982. Le Villafranchien de la région de Teruel (Espagne). Stratigraphie Deformations Milieux. Colloque "Le Villafranchien méditerranéen", Lille, pp. 229–253.

Moissenet, E., 1983. Aspectos de la Neotectónica en la Fosa de Teruel. In: Comba, J.A. (Ed.), Geología de EspañaLibro Jubilar J.M. Ríos vol. 2. IGME, Madrid, pp. 427–446.

Montenat, C., Barrier, P., d'Estevou, P.O., Hibsch, C., 2007. Seismites: an attempt at critical analysis and classification. Sedimentary Geology 196, 5–30.

Moretti, M., 2000. Soft-sediment deformation structures interpreted as seismites in middle-late Pleistocene aeolian deposits (Apulian foreland, southern Italy). Sedimentary Geology 135, 167–179.

Moretti, M., Ronchi, A., 2011. Liquefaction features interpreted as seismites in the Pleistocene fluvio-lacustrine deposits of the Neuquén Basin (northern Patagonia). Sedimentary Geology 235, 200–209.

Moretti, M., Sabato, L., 2007. Recognition of trigger mechanisms for soft-sediment deformation in the Pleistocene lacustrine deposits of the Sant'Arcangelo Basin (southern Italy): seismic shock vs. overloading. Sedimentary Geology 196, 31–45.

Moretti, M., Van Loon, A.J., 2014. Restrictions to the application of 'diagnostic' criteria for recognizing ancient seismites. Journal of Palaeogeography 3 (2), 162–173.

Moretti, M., Alfaro, P., Caselles, O., Canas, J.A., 1999. Modelling seismites with a digital shaking table. Tectonophysics 304, 369–383.

Moretti, M., Soria, J.M., Alfaro, P., Walsh, N., 2001. Asymmetrical soft-sediment deformation structures triggered by rapid sedimentation in turbiditic deposits (late Miocene, Guadix Basin, southern Spain). Facies 44, 283–294.

Obermeier, S.F., 1996. Use of liquefaction-induced features for paleoseismic analysis - an overview of how seismic liquefaction features can be distinguished from other features and how their regional distribution and properties of source sediment can be used to infer the location and strength of Holocene paleo-earthquakes. Engineering Geology 44 (1–4), 1–76.

Obermeier, S.F., Gohn, G.S., Weems, R.E., Gelinas, R.L., Rubin, M., 1985. Geologic evidence for recurrent moderate to large earthquakes near Charleston, South Carolina. Science 277, 408–410.

Ogg, J.G., 2012. Chapter 5: Geomagnetic Polarity Time Scale. In: Gradstein, F.M., Ogg, J.G., Schmitz, M.D., Ogg, G.M. (Eds.), The Geologic Time Scale. Elsevier, Amsterdam.

Opdyke, N., Channell, J.E., 1996. Magnetic Stratigraphy 64. Academic Press, San Diego.

Opdyke, N., Mein, P., Lindsay, E., Pérez-González, A., Moissenet, E., Norton, V.L., 1997. Palaeogeography, Palaeoclimatology, Palaeoecology 133, 129–148.

Osete, M.L., Palencia, A., 2006. Polos paleomagnéticos de los últimos 300 millones de años. Física de la Tierra 18, 157–181.

Owen, G., 1987. Deformation Processes in Unconsolidated Sands. In: Jones, M.E., Preston, R.M.F. (Eds.), Geological Society Spec. Publ. 29, pp. 11–24.

Owen, G., Moretti, M., 2008. Determining the origin of soft-sediment deformation structures: a case study from upper carboniferous delta deposits in south-west wales, UK. Terra Nova 20, 237–245.

Owen, G., Moretti, M., 2011. Identifying triggers for liquefaction-induced soft-sediment deformation in sands. Sedimentary Geology 235, 141–147.

Owen, G., Moretti, M., Alfaro, P., 2011. Recognising triggers for soft-sediment deformation: current understanding and future directions. Sedimentary Geology 235, 133–140.

Peña, J.L., Gutiérrez, M., Ibáñez, M.J., Lozano, M.V., Rodríguez, J., Sánchez, M., Simón, J.L., Soriano, M.A., Yetano, L.M., 1984. Geomorfología de la Provincia de Teruel. Instituto de Estudios Turolenses, Teruel.

Posamentier, H.W., Allen, G.P., 1999. Siliciclastic Sequence Stratigraphy: Concepts and Applications. SEPM Concepts in Sedimentology and Paleontology 7, Tulsa.

Pueyo, E., Garcés, M., Mauritsch, H.J., Lewis, C., Scholger, R., Sancho, C., Molina, R., Schnepp, E., Larrasoaña, J.C., Parés, J.M., Pocoví, A., Muñoz, A., Valero, B., Millán, H., Laplana, C., Oliva, B., González, P., 2006. Sampling, Transportation and Magnetic-Free Consolidation of extremely Soft Sediments for Paleomagnetic Purposes: a Successful ¿Recipe? In: Calvo, M., Garcés, M., Gomes, C., Larrasoaña, J., Pueyo, E., Villalaín, J. (Eds.), Paleomagnetismo en la Península Ibérica: MAGIBER I, Burgos, pp. 119–126.

Ramón, M.J., 2013. Flexural unfolding of complex geometries in fold and thrust belts using paleomagnetic vectors. Unpublished PhD University of Zaragoza, 228 pp. http://zaguan.unizar.es/record/11750

Ramón, M.J., Pueyo, E.L., 2012. Automatic Calculation of Demagnetization Intervals; a New Approach Based on the Virtual Directions Method and Comparison with the Linearity Spectrum Analysis. In: Fernández, L.P., Fernández, A., Cuesta, A., Bahamonde, J.R. (Eds.), GeoTemas 13. Resúmenes Extendidos Del VIII Congreso Geológico de España, Oviedo, pp. 1180–1183.

Rodríguez-López, J.P., Meléndez, N., Soria, A.R., Liesa, C.L., Van Loon, A.J., 2007. Lateral variability of ancient seismites related to diferences in sedimentary facies (the synrift Escucha formation, mid-cretaceous, eastern Spain). Sedimentary Geology 201, 461–484.

Rodríguez-Pascua, M.A., Calvo, J.P., De Vicente, G., Gómez-Gras, D., 2000. Soft-sediment deformation structures interpreted as seismites in lacustrine sediments of the Prebetic zone, SE Spain, and their potential use as indicators of earthquake magnitudes during the late Miocene. Sedimentary Geology 135, 117–135.

Rubio, J.C., Simón, J.L., 2007. Tectonic subsidence vs. erosional lowering in a controversial intramontane depression: the Jiloca basin (Iberian chain, Spain). Geological Magazine 144, 1–15.

Shibuya, H., Merril, D., Hsu, V., Leg, 124, Shipboard Scientific Party, 1991. Paleogene Counterclockwise Rotation of the Celebes Sea-Orientation of ODP Cores Utilizing the Secondary Magnetization. In: Silver, E.A., Rangin, C., von Breymann, M.T. (Eds.), Proceedings of the Ocean Drilling Program. Scientific Results 124, pp. 519–522.

Simón, J.L., 1982. Compresión Y distensión Alpinas en la Cadena Ibérica Oriental PhD. Thesis Universidad de Zaragoza. Publ. Instituto de Estudios Turolenses, Teruel.

Simón, J.L., 1983. Tectónica Y neotectónica Del Sistema de Fosas de Teruel 69 pp. 21–97 Teruel. Q15

Simón, J.L., Arlegui, L.E., Lafuente, P., Liesa, C.L., 2012. Active extensional faults in the central-eastern Iberian chain, Spain. Journal of Iberian Geology 38, 127–144.

Simón, J.L., Arlegui, L.E., Ezquerro, L., Lafuente, P., Liesa, C.L., 2014. Aproximación a la peligrosidad sísmica en la ciudad de Teruel asociada a la falla de Concud (NE España). Geogaceta 5, 7–10.

Simón, J.L., Arlegui, L.E., Ezquerro, L., Lafuente, P., Liesa, C.L., Luzón, A., 2015. Enhaced paleoseismic succession at the Concud fault (Iberian chain, Spain): new insights for seismic hazard assessment. Natural Hazards. http://dx.doi.org/10.1007/s11069-015-2054-6.

Simón, J.L., Arlegui, L.E., Ezquerro, L., Lafuente, P., Liesa, C.L., Luzón, A., 2016. Structure and paleoseismology of the Teruel fault: dynamic interaction and strain partitioning with the Concud fault (eastern Iberian chain, Spain. Journal of Structural Geology (in press).

Sims, J.D., 1975. Determining earthquake recurrence intervals from deformational structures in young lacustrine sediments. Tectonophysics 29, 141–152.

Sinusía, C., Pueyo, E.L., Azanza, B., Pocoví, A., 2004. Datación magnetoestratigráfica del yacimiento paleontológico de Puebla de Valverde (Teruel). GeoTemas 6 (4), 339–342.

Soria, A.R., Muñoz, A., Liesa, C.L., Luzón, A., Meléndez, A., Meléndez, M.N., 2013. Climate-driven cyclicity in an early cretaceous synrift lacustrine series (Aguilón sub-basin, NE Spain). Terra Nova 24, 407–416.

Spalluto, L., Moretti, M., Festa, V., Tropeano, M., 2007. Seismically-induced slumps in lower-Maastrichtian peritidal carbonates of the Apulian platform (southern Italy). Sedimentary Geology 196, 81–98.

Stárková, M., Martínek, K., Mikuláš, R., Rosenau, N., 2015. Types of soft-sediment deformation structures in a lacustrine Ploužnice member (Stephanian, Gzhelian, Pennsylvanian, bohemian massif), their timing, and possible trigger mechanism. International Journal of Earth Sciences 104, 1277–1298.

Stokking, L.B., Musgrave, R.J., Bontempo, D., Autio, W., 1993. Handbook for shipboard Paleomagnetists. ODP tech. Note, 18: College Station, TX (ocean drilling program). http://www-odp.tamu.edu/publications/tnotes/tn18/f_pal.htm.

Thibal, J., Etchecopar, A., Pozzi, J.P., Barthès, V., Pocachard, J., 1999. Comparison of magnetic and gamma ray logging for correlations in chronology and lithology: example from the Aquitanian Basin (France). Geophysical Journal International 137, 839–846.

Tuttle, M.P., Schweig, E.S., Sims, J.D., Lafferty, R.H., Wolf, L.W., Haynes, M.L., 2002. The earthquake potential of the New Madrid seismic zone. Bulletin of the Seismological Society of America 92, 2080–2089.

Van Alstine, D.R., Butterworth, J.E., 1993. Paleomagnetic orientation of fractures and bedding in Rotliegend and Zechstein cores from the southern Permian Basin, North Sea. AAPG Bulletin 77, 1672.

Van Alstine, D.R., Butterworth, J.E., Willemse, E.J.M., Van de Graaff, W.J.E., 1991. Paleomagnetic core-orientation for characterizing reservoir anisotropy: case histories from fractured reservoirs in Abu Dhabi and Venezuela. AAPG Bulletin 75, 687.

van Dam, J.A., 2006. Geographic and temporal patterns in the late Neogene (12-3 Ma) aridification of Europe: the use of small mammals as paleoprecipitation proxies. Palaeogeography, Palaeoclimatology, Palaeoecology 238, 190–218.

van Dam, J.A., Alcalá, L., Alonso-Zarza, A.M., Calvo, J.P., Garcés, M., Krijgsman, W., 2001. High-resolution late Miocene mammal biochronology and paleoecology of the Teruel–Alfambra region (NE Spain). Journal of Vertebrate Paleontology 21, 367–385.

Van der Voo, R., Watts, D.R., 1978. Paleomagnetic results from igneous and sedimentary rocks from the Michigan Basin borehole. Journal of Geophysical Research 83, 5844–5848.

Van Loon, A.J., 2009. Soft-sediment deformation structures in siliciclastic sediments: an overview. Geologos 15, 3–55.

Van Loon, A.J., Brodzikowski, K., Zielinski, 1995. Shock-induced resuspension deposits from a Pleistocene proglacial lake (Kleszczów graben, Central Poland). Journal of Sedimentary Research A65 (2), 417–422.

Vandamme, D., 1994. A new method to determine paleosecular variation. Physics of the Earth and Planetary Interiors 85, 131–142.

Weerd, A., 1976. Rodent Faunas of the Mio-Pliocene Continental Sediments of the Teruel Alfambra Region, Spain PhD. Thesis Utrecht Micropaleontol. Bulletin, Special Publication 2, Utrecht.

Zhang, F.Q., Song, J.S., Shen, Z.Y., Chen, H.L., Dong, C.W., Pang, Y.M., Shu, P., 2007. A study on fracture orientation and characteristic of remnant magnetization of deep-burial volcanic rocks, north of the Songliao Basin. Chinese Journal of Geophysics 50 (4), 1011–1017.